Neurobiology of Disease

# Anti-Inflammatory Modulation of Microglia via CD163-Targeted Glucocorticoids Protects Dopaminergic Neurons in the 6-OHDA Parkinson's Disease Model

Noemie Tentillier,[1,2] Anders Etzerodt,[2] Mads N. Olesen,[1,2] F. Sila Rizalar,[1,2] Jan Jacobsen,[3] Dirk Bender,[3] Søren K. Moestrup,[2,4] and Marina Romero-Ramos[1,2]

[1]CNS Disease Modeling Group, NEURODIN, [2]Department of Biomedicine, and [3]Department of Clinical Medicine, PET Center, Aarhus University Hospital, DK-8000 Aarhus C, Denmark, and [4]Department of Cancer and Inflammation Research, Syddansk University, DK-5000 Odense, Denmark

**Increasing evidence supports a decisive role for inflammation in the neurodegenerative process of Parkinson's disease (PD). The immune response in PD seems to involve, not only microglia, but also other immune cells infiltrated into the brain. Indeed, we observed here the infiltration of macrophages, specifically CD163+ macrophages, into the area of neurodegeneration in the 6-hydroxydopamine (6-OHDA) PD model. Therefore, we investigated the therapeutic potential of the infiltrated CD163+ macrophages to modulate local microglia in the brain to achieve neuroprotection. To do so, we designed liposomes targeted for the CD163 receptor to deliver dexamethasone (Dexa) into the CD163+ macrophages in the 6-OHDA PD model. Our data show that a fraction of the CD163-targeted liposomes were carried into the brain after peripheral intravenous injection. The 6-OHDA-lesioned rats that received repeated intravenous CD163-targeted liposomes with Dexa for 3 weeks exhibited better motor performance than the control groups and had minimal glucocorticoid-driven side effects. Furthermore, these animals showed better survival of dopaminergic neurons in substantia nigra and an increased number of microglia expressing major histocompatibility complex II. Therefore, rats receiving CD163-targeted liposomes with Dexa were partially protected against 6-OHDA-induced dopaminergic neurodegeneration, which correlated with a distinctive microglia response. Altogether, our data support the use of macrophages for the modulation of brain neurodegeneration and specifically highlight the potential of CD163-targeted liposomes as a therapeutic tool in PD.**

*Key words:* CD163; dexamethasone; dopamine; macrophages; microglia; Parkinson's disease

### Significance Statement

**The immune response now evident in the progression of Parkinson's disease comprises both local microglia and other immune cells. We provide evidence that CD163+ macrophages can be a target to modulate brain immune response to achieve neuroprotection in the 6-hydroxydopamine model. To do so, we targeted the CD163+ population, which to a low but significant extent infiltrated in the neurodegenerating area of the brain. Specially designed liposomes targeted for the CD163 receptor were loaded with glucocorticoids and injected peripherally to modify the infiltrated CD163 cells toward an anti-inflammatory profile. This modification of the CD163 population resulted in a distinctive microglial response that correlated with decreased dopaminergic cell death and better motor performance.**

## Introduction

Parkinson's disease (PD) is characterized by the progressive loss of dopaminergic neurons in the substantia nigra (SN) and the presence of intraneuronal aggregated $\alpha$-synuclein in the Lewy bodies. It has been proposed that the immune system plays an active part in the symptoms and progression of PD (Doorn et al.,

Received May 21, 2016; revised June 22, 2016; accepted July 13, 2016.

Author contributions: N.T., A.E., and M.R.-R. designed research; N.T., A.E., M.N.O., F.S.R., J.J., and M.R.-R. performed research; D.B. and S.K.M. contributed unpublished reagents/analytic tools; N.T., A.E., and M.R.-R. analyzed data; N.T., A.E., S.K.M., and M.R.-R. wrote the paper.

This work was supported by the Michael J. Fox Foundation for Parkinson's Disease (M.R.-R.) and the Bjarne Saxhofs Fund administered through the Danish Parkinson's Foundation (M.R.-R.). N.T. was a recipient of a doctoral fellowship from the Aarhus University. We thank Gitte Toft Ulbjerg and Zane Binate for excellent technical support.

S.K.M. owns shares in Affinicon, which holds IP protecting the use of CD163 drug targeting. The remaining authors declare no competing financial interests.

Correspondence should be addressed to Marina Romero-Ramos, Department of Biomedicine, Wilhem Meyers Alle 4, Aarhus University, Aarhus C DK-8000, Denmark. E-mail: mrr@biomed.au.dk.

F. S. Rizalar's present address: Molecular Biology and Genetics Department, Koç University, Rumeli Feneri Yolu, Istanbul 34450, Turkey.

DOI:10.1523/JNEUROSCI.1636-16.2016

Copyright © 2016 the authors 0270-6474/16/369375-16$15.00/0

2012; Blandini, 2013). Supporting this, epidemiological studies show that the use of nonaspirin NSAIDs decreases the risk of developing PD (Rees et al., 2011) and genetic studies described a significant association between polymorphisms in the HLA gene loci and the risk for late-onset PD (Hamza et al., 2010; International Parkinson Disease Genomics Consortium, 2011).

Microgliosis in PD brain has been shown repeatedly in patients and has also been observed in animal models of PD (Cebrián et al., 2015). PET brain imaging and postmortem studies in PD shows early but sustained microglia activation that was not only limited to areas with significant neuronal death, but was also correlated with α-synuclein pathology (Hunot et al., 1996; Knott et al., 2000; Imamura et al., 2003; Croisier et al., 2005; Ouchi et al., 2005; Gerhard et al., 2006). Importantly, α-synuclein released from neurons acts as a proinflammogen on microglia, further contributing to the microgliosis (Sanchez-Guajardo et al., 2013a). The microglia response is complex, as shown by the variety of proteins upregulated, such as MHC-II, CD68 (Banati et al., 1998; Croisier et al., 2005), COX2, and iNOS (Hunot et al., 1996; Knott et al., 2000). The immune response is also noticed in periphery and involves both pro-inflammatory signals such as TNF and IL-1b, but also anti-inflammatory molecules such as IL-4 and IL-10, all of which are increased in the serum and/or CSF of PD patients (Mogi et al., 1994; Garcia-Esparcia et al., 2014). This widespread and chronic inflammatory reaction in PD patients suggests that microglia fail to solve the insult that triggers their activation and such maintained chronic activation might lead to neuronal death (Herrera et al., 2005; Joers et al., 2016).

The immune response in PD patients and in animal PD models seems to involve, not only microglia, but also infiltrated peripheral macrophages (Zhao et al., 2011) and lymphocytes (Lossinsky and Shivers, 2004; Brochard et al., 2009). It has been proposed that CD4 T cells may play a key role in the dopaminergic cell death in the MPTP and the α-synuclein PD models (Brochard et al., 2009; Sanchez-Guajardo et al., 2013b). Further supporting a role of peripheral cells, unrelated inflammatory peripheral events increase neurodegeneration in PD models (Villaran et al., 2010; Gao et al., 2011).

Synthetic glucocorticoids are the most potent known drugs used to relieve inflammation. Among them, dexamethasone (Dexa) was shown previously to be neuroprotective in the MPTP mouse PD model (Kurkowska-Jastrzebska et al., 2004) and in an LPS rat PD model (Castaño et al., 2002). However, chronic treatment with Dexa and glucocorticoids are well known to induce serious side effects, so we used a low-dose Dexa-targeted approach. We have shown previously that both *in vitro* and *in vivo*, anti-CD163-Dexa-conjugate attenuated the LPS-induced inflammatory response in rats (Graversen et al., 2012). CD163 is a hemoglobin scavenger receptor (Kristiansen et al., 2001) expressed in monocytes/macrophages that has been involved in different inflammatory diseases (Etzerodt and Moestrup, 2013; Dultz et al., 2016; Liu et al., 2015). In the brain, CD163 is expressed in perivascular macrophages (PVMs) but not in microglia, so it constitutes a potential marker for infiltrated peripheral immune cells in the brain parenchyma (Polfliet et al., 2006).

Microgliosis and increased pro-inflammatory mediators in brain are also found in the 6-hydroxydopamine (6-OHDA) PD model (Cicchetti et al., 2002; Nagatsu and Sawada, 2005; McCoy et al., 2006; Na et al., 2010). In the present study, we investigated macrophage infiltration in the brains of 6-OHDA-lesioned rats and tested whether anti-inflammatory modulation of infiltrating macrophages protects against neurodegeneration.

## Materials and Methods

*Animals*. Adult female Sprague Dawley rats ($n = 120$; Taconic) weighing 225–250 g at the time of the surgery were housed two per cage with *ad libitum* access to food and water in a climate-controlled facility under 12:12 h light/dark cycle. The animal experiments were conducted under humane conditions with ethical approval from the Danish Animal Inspectorate that adheres to the European Rules.

*Dopaminergic lesion*. Rats were anesthetized with medetomidine hydrochloride (1 mg/ml) diluted 1/15 in fentanyl (50 μg/ml) (1.6–1.8 ml/injection, i.p.) and placed in a stereotaxic apparatus (Stoeling). The skull was exposed by an incision in the midline and three 2 mm holes were drilled to allow 2 μl injections of 6-OHDA (7 μg in saline and 0.02% ascorbic acid) per site or vehicle for sham injections. The solution was injected over 2.5 min using a 5 μl Hamilton syringe attached to a glass capillary (outer diameter of 60–80 μm) at the following coordinates (in mm): AP +1.0; 0,0; −1.0 and ML ±3.0; ±3.4; ±4.2 from bregma and −4.9 ventral from dura (nose bar at −3.3) according to the atlas of Paxinos and Watson (Paxinos and Watson, 1998). After the injection, the cannula was left in place for 5 min before slow retraction. Animals were sutured using metal clips and injected with buprenorphine (0.36 mg/kg) for pain relief and awakened with a single injection of antipamezole hydrochloride (0.7 mg/kg). Fully awakened animals were placed back in their cages.

The 6-OHDA (Sigma-Aldrich) was dissolved at 4.2 mg/ml (the 6-OHDA used contains 82% free base) with 0.02% ascorbic acid in sterile saline, kept on ice for no more than 2 h, and protected from light throughout the entire procedure. For sham injections, 0.02% ascorbic acid in sterile saline was used.

*Liposome preparation*. Liposomes were prepared and modified for CD163 targeting as described previously (Etzerodt et al., 2012). In short, liposome formulations were formed using the ethanol injection method from a mixture of hematopoietic stem/progenitor cells Hydrogenated soy L-α-phosphatidylcholine, cholesterol, and mPEG2000-PE (molar ratio of 55:40:5; Lipoid and Sigma-Aldrich). Lipids were dissolved in 100 μl of EtOH at 65°C for 10 min, followed by hydration for 1 h at 65°C in 900 μl of aqueous buffer. Liposomes were sized by extrusion 25 times through a 0.1 μm filter using a mini-extruder kit (Avanti Polar Lipids) and dialyzed against 150 mM NaCl (0.9% NaCl) overnight at 4°C. Lipid content, drug content, and encapsulation efficiency were estimated from high-pressure size-exclusion chromatography (UV absorbance 210 nm) using a Dionex UltiMate 3000 HPLC system (Thermo Scientific) equipped with an Ascentis C18 column (Sigma-Aldrich). Liposome sizes were estimated using dynamic light scattering and the DynaPro NanoStar system (Wyatt Technology). Modification of liposomes for CD163 targeting was done as described previously by the postinsertion method of lipidated antibody using the CD163-antibody clone ED2 (AbD Serotec) (Torchilin et al., 2001; Etzerodt et al., 2012).

For liposomes encapsulating calcein, lipids were rehydrated in 250 mM calcein disodium (Sigma Aldrich) and 150 mM NaCl and dialysis was repeated five times to remove excess calcein. Liposomes encapsulating Dexa-21-hemisuccinate lipids were rehydrated in 200 mM $CaAcO_2$ and remote loading of Dexa was done using the remote loading technique for amphiphatic weak acids (Clerc and Barenholz, 1995) with a Dexa to lipid ratio of 1:10 (mol/mol). Formulation of liposomes encapsulating $^{125}$I-labeled Bolton–Hunter reagent was done by rehydrating lipids in a 80 mM HBS buffer (80 mM HEPES, 150 mM NaCl), pH 8.6, supplemented with 80 mM L-arginine (Mougin-Degraef et al., 2006). On the day of injection, L-arginine-containing liposomes were radioactively labeled by incubating liposomes for 30 min at room temperature with $^{125}$I-Bolton–Hunter reagent (0.48 MBq/μmol lipid) in 5 mM CBS (5 mM citrate, pH 5.0, 150 mM NaCl). Excess $^{125}$I–Bolton–Hunter reagent was subsequently removed using a Zeba Spin desalting column (7 K MWCO; Thermo Fisher Scientific).

*Biodistribution of radioactive CD163 liposomes*. Three weeks after striatal injections, 6-OHDA or sham ($n = 4$ per group) rats were anesthetized with 2.5% isoflurane (IsoVet 1000 mg/g inhalation vapor, liquid; Chanelle) in 0.4 L/min $O_2$ and 1 L/min $N_2O$ that was maintained during the intraveous injections. A single intravenous, 0.5 ml injection of $^{125}$I-

anti-CD163-liposomes (0.125 mM liposome solution, $1.5 \times 10^6$ cpm/animal, $n = 8$) was administered to each animal. Blood samples were collected from the sublingual vein at several time points after liposome injection (2, 20, 40, and 60 min). Rats were killed after 2 h by cervical dislocation under anesthesia, at which time a final intracardiac blood sample was taken and selected organs were rapidly dissected (heart, two distant pieces of the spleen, liver, and both kidneys), weighed, and analyzed for $^{125}$I radioactivity using an alpha-counter (COBRA 5002; PerkinElmer). The radioactivity results were adjusted to the mass of tissue and are presented as a percentage of the total injected dose for each organ. Time course of the blood clearance of $^{125}$I was determined in 0.5 ml of blood and is presented as relative radioactive emission compared with emission 2 min after $^{125}$I-anti-CD163 injection.

*Tracking of peripherally injected liposomes*. One and 3 weeks after surgery (6-OHDA; $n = 4$ and sham; $n = 2$), lesioned and naive ($n = 2$) rats received a single intravenous injection of CD163-targeted calcein-loaded liposomes (ED2-LCL-Calcein; dose lipid = 1.25 mM and IgG = 0.075 mg/ml, injection volume = 2 ml/kg) under isoflurane anesthesia (same procedure as above). Eighteen hours after ED2-LCL-Calcein injection, all animals were killed and their brains perfused, sliced, and processed for immunofluorescence to detect the presence of calcein in CD11b+ cells (see below).

*Isolation of peritoneal macrophages*, *selection*, *and* ex vivo *loading*. Peritoneal macrophages were collected from 8- to 10-week-old naive rats by repeated PBS peritoneal lavage. The cell suspension obtained was centrifuged for 10 min at $300 \times g$, the supernatant discarded, and the cell pellet resuspended in RPMI (RPMI 1640 w/L-glutamine medium, Lonza) complete medium (RPMI-CM: 10% heat-inactivated FCS; Thermo Fisher Scientific) and 1% HEPES (Invitrogen). Cells were stained and processed for FACS sorting of the CD11b+/CD163+ population with FACSAria III sorters (BD Biosciences). Thereafter, the cells were briefly kept in complete RPMI 1640 (Lonza) medium containing penicillin (100 U/ml; Thermo Fisher Scientific)/streptomycin (100 U/ml; Thermo Fisher Scientific) and 10% FCS (Thermo Fisher Scientific) at 37°C and 5% $CO_2$ until proceeding with Qdot loading and *in vivo* injection.

Sorted CD11b+/CD163+ peritoneal macrophages were loaded with fluorescent Qdot565 following the protocol from the Qtracker565 cell-labeling kit provided by the manufacturer (Thermo Fisher Scientific). Briefly, 10 nM labeling solution was prepared from premixed solutions and incubated for 5 min at room temperature. Then, fresh complete RPMI was added to the solution and vortexed for 30 s. Thereafter, a sample containing $10^6$ cells (from a cell suspension at $\sim 1 \times 10^7$ cells/ml in RPMI) was added to the labeling solution and incubated for 45 min at 37°C, followed by 2 washes with complete RPMI. The resulted cell suspension was maintained at room temperature until being injected into the animals.

*Flow cytometry*. Freshly isolated cells were processed for flow cytometry analysis within 2 h after the harvesting time. All incubations were performed on ice and all washes (100 μl, 300 g, 5 min, 4°C) and antibody mixing were done in FACS buffer (1% FCS; 5% EDTA, 50 mM; Sigma-Aldrich); 1% penicillin/streptomycin (Invitrogen), in 1× PBS (Invitrogen). Cell number and viability were assessed using cell counter (Moxi, Z Mini automated cell counter; Orflo). Then $2 \times 10^6$/100 μl cell suspensions were distributed in Trucount Tubes (BD Biosciences) and washed twice. The cells were then blocked for 10 min in 5% BSA in FACS buffer, washed afterward, and stained with single antibody or antibody solution for 10 min in the dark using CD11b-FITC (Clone OX-42; AbD Serotec) and CD163-AF647 (Clone ED2; AbD Serotec). The optimal concentration of each antibody was determined by titration in preliminary experiments. For each sample, we included unstained cells for negative controls and each antibody's respective isotype control. Thereafter, cells were washed twice and kept in FACS buffer for analysis. Sample data and cell sorting were processed with FACSAria III sorters (BD Biosciences). All samples were gated first on live cells according to their forward scatter (FSC)/side scatter (SSC) and doublets were removed by plotting data for height (H) and area (A): FSC-H/FSC-A and SSC-H/SSC-A. After cell sorting, cells were collected in 50% FCS in PBS.

*CD163-targeted Dexa-loaded liposome treatment*. The rats were divided into four groups, all receiving the first treatment injection in tail vein 1 d before brain surgery, followed by three weekly injections for 3 weeks. The experimental group of animals received 0.02 mg Dexa/kg encapsulated in liposomes coated with anti-CD163-antibody (referred to hereafter as ED2-LCL-Dexa). In addition, control groups included: (1) rats receiving PBS in nontargeted liposomes (lipid dose: 0.125 mM, referred to as: Lip-PBS); (2) rats receiving free Dexa (1.0 mg Dexa/kg, standard high dose according to the literature; Graversen et al., 2012); and (3) rats receiving Dexa encapsulated in nontargeted liposomes (0.02 mg Dexa/kg, referred to hereafter as LCL-Dexa). For all injections, the rats were briefly anesthetized with 2.5% isoflurane mixed with 0.4 L/min $O_2$ and 1 L/min $N_2O$ and liposome preparations were injected slowly through the tail vein at a volume of 2 ml/kg animal body weight.

*Behavioral test*. In the second week after striatal lesion, locomotor asymmetry was evaluated using a modified version of the cylinder test originally described (Schallert et al., 2000). Briefly, the animals are placed in a transparent Plexiglas cylinder (height 30 cm, diameter 20 cm), with two mirrors placed behind to visualize the cylinder surface fully. Spontaneous use of the animal forepaws (independently or simultaneously) was video recorded and a total of 20 forepaw touches were counted. Each animal was coded so that the researcher analyzing the video was blinded to the identity of the animal. The animals were tested only once and, after 2–10 min inside the cylinder, were required to achieve the desired number of touches. The left paw touches were expressed as a percentage of total forelimb touches. For data quality, a second observer scored a random sample of 20% of the animals and the data between the two observers were compared for variability (Pearson $r = 0.081$). In addition, an unrelated researcher verified the accuracy of data transfer from the laboratory notebooks to the electronic files.

*Perfusion and tissue processing*. Rats were killed 1 and 3 weeks after surgery with an overdose of pentobarbital (50 mg/kg, i.p.). On respiratory arrest, they were perfused through the ascending aorta with ice-cold saline, followed by 4% ice-cold paraformaldehyde (PFA; in 0.1 M NaPB, pH 7.4). When relevant and before PFA perfusion, blood was collected and the heart, thymus, liver, and/or spleen were dissected and frozen in dry ice for storage at −80°C. PFA-perfused brains were postfixed in the same PFA solution for 2 h, transferred to 25% sucrose solution (in 0.02 M NaPB), sliced into 40-μm-thick coronal sections (Microm HM 450; Brock and Michelsen), separated in serial sections (series of 8 for the striatum and 6 for the SN), stored at −20°C.

For selected experiments, animals were deeply anesthetized using isoflurane and killed by cervical dislocation. Thereafter, selected organs were dissected, frozen in dry ice, and kept at −80°C until use.

*Immunohistochemistry*. Immunohistochemical stainings were performed on free-floating brain sections as described previously (Febbraro et al., 2013) using the following mouse primary antibodies: tyrosine hydroxylase (TH; 1:3000; Millipore), CD11b (Mac1; 1:500; AbD Serotec), CD163 (ED2; 1:1000; AbD Serotec), CD68 (ED1; 1:200; AbD Serotec), and MHCII (OX-6; 1:250; AbD Serotec). The sections stained with CD11b antibody were counterstained with cresyl violet (0.5% solution) before coverslipping. Bright-field images were acquired with a Leica DMI600B microscope.

For immunofluorescence, CD11b (Mac1; 1:500; AbD Serotec) primary antibody incubation was followed by several washes and incubated with species-specific fluorophore-conjugated antibodies (Alexa-Fluor 647 and Alexa-Fluor 568; Invitrogen) in 0.25% Triton X-100 in KPBS with 2.5% horse serum at room temperature for 2 h and DAPI (1: 2000; Sigma-Aldrich) was added for the last 10 min for nuclear staining. After final washes, sections were mounted and confocal images were obtained using an LSM 710 Meta confocal microscope (Zeiss) with a 63× lens.

*Microscopic analysis and stereological analysis*. The unbiased stereological estimation of the total number of either TH+ or CD11b+ cells in the SN or CD163+ cells in the striatum were made by an observer blinded to the identity of the animal using the optical fractionator principle (Westermeyer, 1991). This sampling technique is not affected by tissue volume changes and does not require reference volume determinations. Samplings were performed using the NewCast module in VIS software (Visiopharm). A 1.25× low-power objective on a Leica DMI600B microscope was used to delineate the borders of the SN and striatum based on anatomical morphology. In brief, for the SN cells, every sixth section from the entire SN (typically eight to nine sections in a series per animal), from the rostral tip of the pars compacta to the caudal end of the pars reticulate, was used. For striatum cells, every eighth section from the

entire striatum (typically 10–12 sections in a series per animal), from the rostral tip of the striatum to the level of −1.80 relative to bregma, were used. The actual counting was performed with a 40× objective (numerical aperture 0.75). The counting frame (56.89 μm × 42.66 μm) was placed randomly by the VIS module and moved systematically until the entire delineated region was sampled. The sampling frequency was chosen by adjusting the *X–Y* step length between 190 and 240 μm for CD163 cell counting, between 230 and 280 for CD11b+ cell counting, and between 140 and 280 for TH+ cell counting such that between 100 and 200 cells were counted on each side of the brain for every animal. The estimated total number of positive cells was calculated according to the optical fractionator formula and a coefficient of error of <0.10 was accepted.

For MHCII+ cell counting, one section of the SN from each animal located between −5.60 mm and −6.04 mm from bregma according to the mouse brain atlas (Paxinos and Watson, 1998) was selected and the quantification was made using a bright-field Leica DMI600B microscope at a magnification of 10×.

*Striatal fiber density measurement*. The optical density of TH+ fibers in the striatum was measured at 6 different rostro-caudal levels according to the rat brain atlas (Paxinos and Watson, 1998): AP: +1.60; +1.00; 0.20; −0.30; −0.92; −1.40 mm relative to bregma. The different brain sections were scanned using a densitometer (Bio-Rad GS-710) and the digital images obtained were analyzed by ImageJ software using grayscale. The optical density for each section was corrected for nonspecific background measured from corpus callosum. The data are presented as a percentage of the lesioned side to the intact control side.

*Analysis of cortisol levels*. Sera were obtained from the collected blood samples by centrifugation 400 × *g* for 15 min at 4°C and the cortisol assay was performed using 1:20 diluted samples. The endogenous cortisol concentrations were measured using the Cortisol Parameter Assay Kit (R&D Systems). Sample dilutions were performed by adding 20 μl of serum sample into 380 μl of calibrator diluent from the kit. The samples were read using a Cobas 6000 analyzer (Roche Diagnostics) with 450 nm wavelengths according to the manufacturer's instructions.

*High-performance liquid chromatography*. At the day of the analysis frozen SN or striata were briefly sonicated (Branson Sonifer 250) on ice in 20 mM Tris-acetate (pH 6.1, 0.05 ml for each 0.01 g tissue weight). Then, 100 μl of tissue homogenate was mixed 1:1 with 0.8 M perchloric acid, incubated on ice for 15 min, diluted with Milli-Q water (Millipore), and centrifuged at 10,600 × *g* for 10 min at 4°C) through a filter with a 0.22 μm pore size (Sigma-Aldrich). Finally, the supernatant was distributed into vials and used for HPLC analysis. The concentrations of dopamine (DA) and its metabolites, DOPAC, HVA, and 3-MT, were determined via HPLC with electrochemical detection. Briefly, 75 μl of sample was injected automatically into the HPLC system and monoamines were separated using a constant flow of 0.5 ml/min by reversed-phase chromatography (MD-150, C18), 150 × 2 mm (3 μm) column (ESA no. 70–4129), using 90 mM sodium dihydrogen phosphate, 14.3 mM triethylamine, 1.7 nM sodium 1-octanesulphonic acid, 50 μM EDTA and 10% acetronitril, pH 3.0, as a mobile phase. Electrochemical detection was accomplished using a coulometric analytical cell (ESA 5014B) and cell potential set at E2 = +250 mV (Coulochem II; ESA). The standard mixture of DA, DOPAC, HVA, and 3-MT was used to identify and quantify each compounds from the animal samples. The final concentration of each monoamine was adjusted to the protein concentration per sample. The protein concentration was determined by bicinchoninic acid assay (BCA). A total of 50 μl of the initial sonicated striatum and SN samples was added to 96-well plate as triplicates. Standards prepared with 0.02% BSA and $ddH_2O$ were also added as triplicates. A total of 200 μl of the bicinchoninic acid/copper sulfate mixture (200 μl of bicinchoninic acid + 4 μl of copper sulfate per well) was added to each well. After the Parafilm-sealed plate was incubated for 1 h at 37°C, protein concentrations were determined using the Protein-Quant (BCA) program in Softmax-Pro Software.

*Statistics*. In all cases, and when the experimental design allowed, the researcher was blinded to the identity of the animal/sample handled or quantified. All data were expressed as mean ± SEM. Statistical analyses were made using GraphPad Prism 6.0 for Mac using one-way ANOVA test followed by Tukey's multiple-comparisons test. When appropriate, paired *t* tests were used. Values of $p < 0.05$ were considered to be significant.

## Results

### 6-OHDA induced degeneration results in the increase of CD163+ cells in striatal parenchyma

The expression of the scavenger receptor CD163 in the brain is limited to meningeal macrophages and the PVM (Polfliet et al., 2006). Therefore, the presence of CD163+ cells in the brain parenchyma may suggest an infiltration of peripheral, meningeal, or PVM cells or an abnormal upregulation of the CD163 expression by the local microglia. To determine whether the CD163+ population changed during the neurodegenerative process occurring in the 6-OHDA rat PD model, we performed stereological quantification of the CD163+ cells in the striatum at 1 and 3 weeks after 6-OHDA surgery. To account for the possible infiltration of CD163+ cells into the striatal parenchyma due to the physical damage induced by the surgery, we performed a sham surgery in the contralateral side. CD163 immunostaining revealed two types of cells: rod cells, which were elongated and typically associated with blood vessels and thus resemble the previously described PVMs (Fig. 1*A′*,*B′*), and polygonal cells that were not associated with blood vessels but located in the parenchyma and consequently might correspond to infiltrating macrophages (Fig. 1*B″*,*B‴*). One-week after surgery, no significant changes in the total number of CD163+ cells were observed between the ipsilateral and contralateral striatum. In the ipsilateral sham striatum, >95% of the CD163+ cells were found mainly as rod cells (PVMs) that were clearly associated with blood vessels (Fig. 1*B*,*C*). Similar results were obtained from the contralateral striata, although with lower numbers of polygonal cells, suggesting a small but nonsignificant increase of CD163+ polygonal cells in the ipsilateral striatum. However, 3 weeks after surgery and 6-OHDA injection, the total number of CD163+ cells was significantly increased in the 6-OHDA lesion striatum (Fig. 1*C*). This increase was due to an elevated number of CD163+ polygonal cells located in the striatal parenchyma compared with the sham contralateral side (22% of total CD163+ cells), suggesting a recruitment of peripheral immune cells to the side of neurodegeneration.

### Peripherally transferred CD163+ cells infiltrate the striatal parenchyma in the 6-OHDA PD model

The stereological data suggest that the CD163+ polygonal cell population is recruited to the brain, specifically to the striatum, upon induction of neurodegeneration using 6-OHDA. To confirm that peripheral CD163+ macrophages could be indeed recruited to the brain parenchyma, CD11b+/CD163+ peritoneal cells were isolated from a group of naive rats (Fig. 2*B*,*C*) labeled with fluorescent Qdot (565 nm) for *in vivo* tracking and injected intravenously in 6-OHDA-lesioned animals 3 weeks after brain surgery. Immunohistochemistry of brain parenchyma for CD11b (expressed by microglia and macrophages) from the rats killed 18 h after intravenous cell transfusion showed Qdot565 nm-positive CD11b+ cells of polygonal body shape in the striatum (Fig. 2*D*), confirming the infiltration of peripheral CD163+ cells to the brain.

### CD163-targeted liposomes target the brain efficiently, especially in the 6-OHDA model

The infiltration of peripheral CD163+ cells into striatum enabled us to use the CD163+ cells as mediators and/or tools to modify the immune environment in the brain of 6-OHDA-injected animals. To do so, we designed long-circulating liposomes (LCLs), which were specifically targeted toward the CD163 receptor, by coating them with an anti-CD163 antibody (ED2

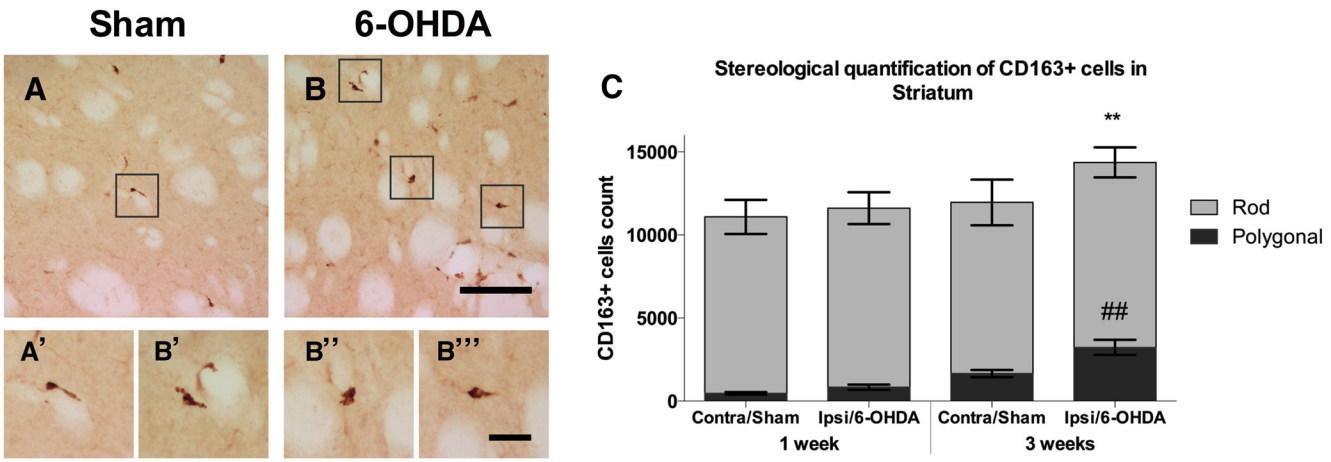



**Figure 1.** CD163+ cells in striatum. ***A***, ***B***, Representative photos of striatum immunostained against CD163 3 weeks after surgery: the contralateral striatum received sham vehicle injection and the ipsilateral side received 3 × 7 $\mu$g of 6-OHDA (see Materials and Methods). CD163+ cells in the contralateral striatum appeared mostly as rod-shaped cells associated with blood vessels (***A′***, ***B′***), whereas the 6-OHDA-lesioned side also exhibited numerous cells of polygonal shape in the parenchyma (***B′′***, ***B′′′***). ***C***, Bar graph showing the average number of the two types of CD163+ cells in the striatum at 1 and 3 weeks after surgery. Stereological quantification of the CD163+ cells in the 6-OHDA-injected striatum 3 weeks after surgery shows a significant increase of total CD163+ cells, which was mainly driven by the increase of polygonal cells in the parenchyma. Values are mean ± SEM ($n = 5$). Paired $t$ test analysis: $^{**}p < 0.001$; $^{\#\#}p < 0.01$.

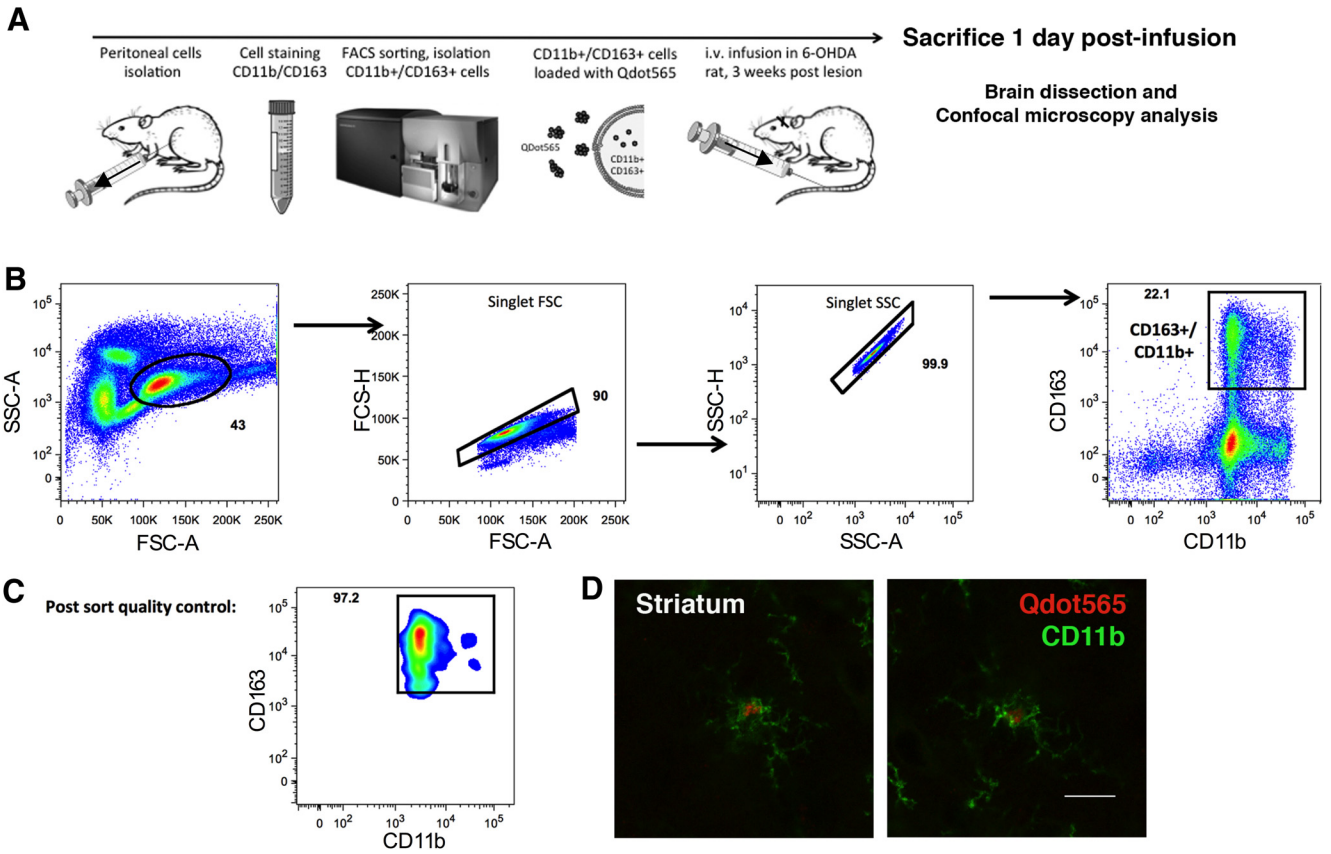



**Figure 2.** Tracking of *ex vivo* fluorescence-labeled CD163+ macrophages in the 6-OHDA model. ***A***, Schematic representation of the experimental design: peritoneal macrophages were isolated from a naive rat and CD11b+/CD163+ cells were FACS sorted. Thereafter, the cells were *ex vivo* loaded with Qdot565 and transfused intravenously to rats 3 weeks after 6-OHDA lesion. The animals were killed 24 h later and the brain processed for immunofluorescence (for details, see Materials and Methods). ***B***, Representative FACS dot plot showing our selection strategy of CD11b+/CD163+ cell population: selection of live cells with FSC and SSC plot, doublets exclusion based on FCS-A/FCS-H and SSC-A/SSC-H, and a final gate based on CD11b and CD163 expression and on isotype controls. ***C***, Sort quality control of CD163+/CD11b+ cells. ***D***, Confocal microscopic analysis showing CD11b+-containing Qdot565 in the brain parenchyma suggesting infiltration of the *ex vivo*-loaded cells. Scale bar, 6 $\mu$m applies to both.

clone). To assess the potential of the ED2-LCLs as drug carriers and to evaluate biodistribution in the 6-OHDA model, we loaded the ED2-LCLs with a $^{125}$I radiolabel and injected a single dose intravenously (~0.03 MBq) in 6-OHDA-lesioned animals and sham rats 3 weeks after brain surgery. We followed the clearance of the radioactive liposomes from the blood circulation, taking regular blood samples for 2 h; thereafter, all animals were killed. We collected brain, spleen, kidneys, heart, and a portion of the

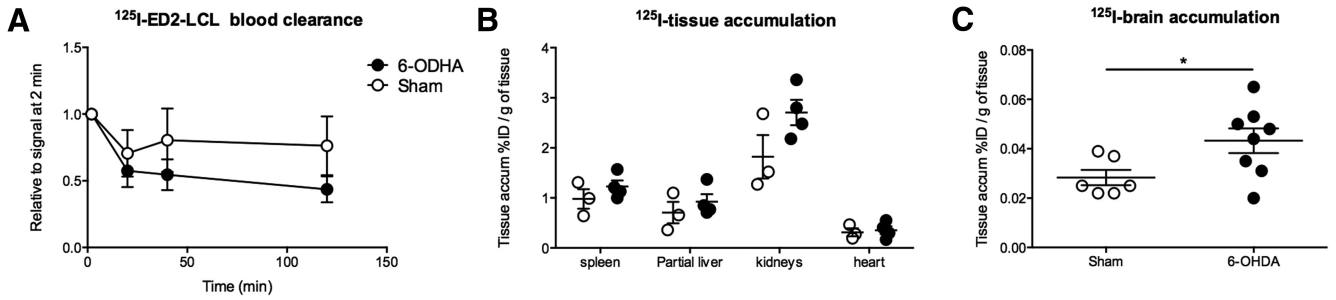



**Figure 3.** Biodistribution of $^{125}$I-radiolabeled-ED2-liposomes injected intravenously in the 6-OHDA model. ***A***, Blood clearance of $^{125}$I-radiolabeled CD163-targeted-liposomes ($^{125}$I-ED2-LCL) at different time points after intravenous injection. Values are expressed as relative to signal at 2 min. ***B***, Mean and individual numbers of the radioactive signal from the $^{125}$I-ED2-LCL taken up in liver, spleen, kidney, and heart. ***C***, Mean and individual numbers of the radioactive signal from the $^{125}$I-ED2-LCL uptaken in brain. In ***B*** and ***C***, values are expressed as a percentage of the injected dose per gram of wet tissue. Values are mean ± SEM ($n = 3$ sham and $n = 4$ 6-OHDA). Unpaired *t* test analysis: $^*p < 0.05$.

liver to quantify the relevant quantity of radioactivity and to calculate the retention of $^{125}$I-radiolabeled ED2-LCLs in these different organs to compare distribution and clearance in both 6-OHDA and sham animals.

The $^{125}$I radiolabel was easily detectable in circulation soon after intravenous injection, but decreased rapidly, with only 55% of the original dose detected in the blood of 6-OHDA-injected rats after 20 min. Thereafter, the levels of radioactivity remained almost stable in the blood until 2 h after injection (Fig. 3*A*). Interestingly, the 6-OHDA-injected animals had always the lowest radioactive readouts in circulation at all time points tested, although these were not significantly different from sham (Fig. 3*A*). When we measured the levels of radioactivity accumulated in tissue after 2 h in selected tissues, we could detect signal in all tissue analyzed, but the highest levels were found in the liver, spleen, and kidneys (Fig. 3*B*). The high radioactivity signal from the kidneys suggests an increased filtration of liposome-free $^{125}$I, which correlates with the suggested increased blood clearance in the 6-OHDA animals. Moreover, compared with sham animals, increased radioactivity levels were also detected in the brains of animals injected with 6-OHDA (Fig. 3*C*), thus confirming the putative potential of these liposomes as therapeutic tools for brain neurodegeneration. The uptake of radioactive liposomes in the brain may be direct; that is, circulating $^{125}$I-radiolabeled ED2-LCLs are taken up by CD163-expressing cells in the brain (likely PVM); or indirect, $^{125}$I-radiolabeled ED2-LCLs are taken up by peripheral CD163+ macrophages, which are then recruited to the brain.

To further confirm the potential of CD163-targeted-LCLs to reach the brain, we injected ED2-LCLs loaded with calcein intravenously in 6-OHDA-lesioned rats 1 and 3 weeks after brain surgery. Subsequent analysis of the brains by confocal microscopy confirmed the uptake of ED2-LCLs in the brain tissue because calcein was observed in CD11b+ cells located in the brain parenchyma (Fig. 4), further supporting the potential of CD163-targeted LCLs as tools to target cells that reach the brain parenchyma. However, we cannot discard at this point that the CD163-targeted LCLs loaded with calcein were taken up by CD163+ PVM because some of the calcein-loaded cells appeared in close proximity to blood vessels (Fig. 4*A–D*).

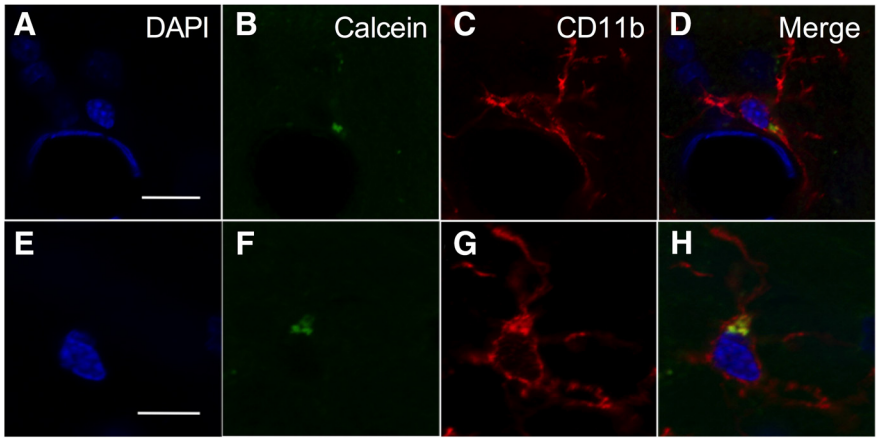



**Figure 4.** Peripheral injection of calcein-loaded ED2 liposomes in the 6-OHDA model. CD11b+ cells loaded with calcein were found in the brain parenchyma, suggesting the uptake of liposomes by infiltrated CD163+ cells and/or PVM. ***A–D***, CD11b+ cells loaded with calcein in proximity of a blood vessel (likely a PVM). ***E–H***, CD11b+ cell loaded with calcein not clearly associated with any blood vessel. Scale bar in ***A***, 11 $\mu$m and applies to top row; scale bar in ***E***, 5.5 $\mu$m and applies to bottom row.

### Experimental design: repeated injections of Dexa encapsulated in liposomes targeted for the CD163 in the PD model

Our data showed that the CD163+ peripheral cells are recruited to the brain, where they infiltrate the striatum of rats in the 6-OHDA model, and that we could access the brain parenchyma using this CD163+ population by specific targeting via ED2-LCLs. Therefore, we designed an experimental approach to use CD163+ cells to modify the neuroinflammatory process in striatum and limit the pro-inflammatory environment in the neurodegenerative area. To do so, we loaded the CD163-targeted LCLs with Dexa with the aim of modifying CD163+ cells toward an anti-inflammatory profile. We hypothesized that these modified infiltrated CD163+ cells would modulate the inflammatory process associated with the 6-OHDA lesion in the striatal parenchyma, resulting in a neuroprotective effect in the nigrostriatal dopaminergic system. Treatment was initiated 1 d before the intracerebral 6-OHDA lesion, followed by treatment 3 times per week for 3 weeks with Dexa-loaded-ED2-LCLs (Dexa 0.02 mg/kg, 0.125 mM liposome solution; ED2-LCLs-Dexa). The following were used as controls: (1) free phosphorylated-Dexa (Dexa 1 mg/kg; free Dexa), (2) Dexa loaded in nontargeted liposomes (Dexa 0.02 mg/kg, 0.125 mM liposome solution; LCL-Dexa), and (3) PBS-loaded liposomes (0.125 mM liposome solution, PBS, 0.15 M NaCl in 10 mM phosphate buffer, pH 7.4; PBS-LCL) in three parallel groups. In a pilot experiment, we confirmed that

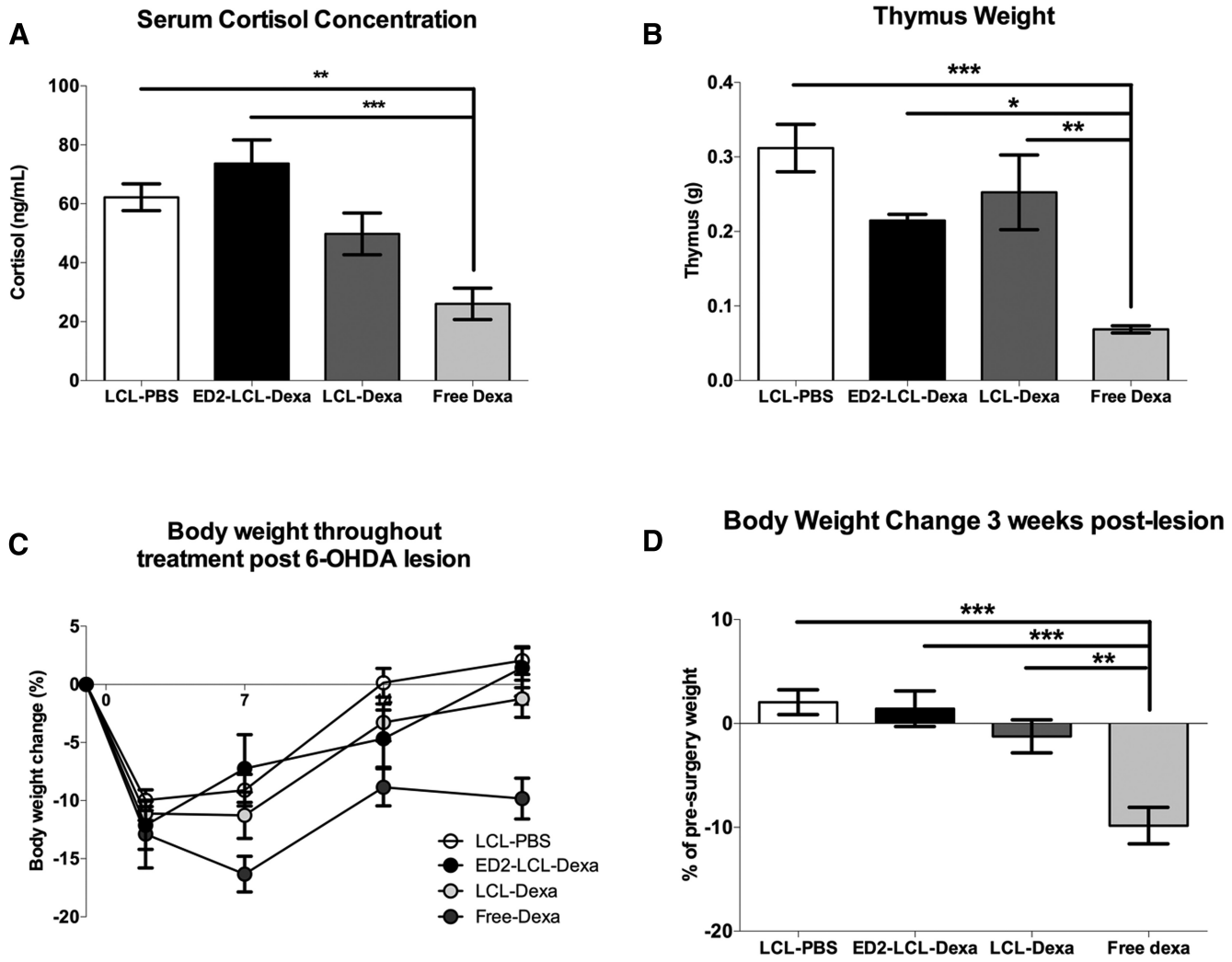



**Figure 5.** Treatment effect in systemic markers. Bar graphs show levels of cortisol in serum and ($n = 6–10$; ***A***) wet thymus tissue weight ($n = 5–6$; ***B***) after 3 weeks of treatment starting 1 d before the 6-OHDA striatal injection. ***C***, ***D***, Body weight changes throughout the 3 weeks of treatment (***C***) and at the end point (***D***) ($n = 7$). ED2-LCL-Dexa treatment was consistently significantly different from free Dexa treatment. Values are mean ± SEM. One-way ANOVA followed by Tukey *post hoc* analysis: ***$p < 0.001$; **$p < 0.01$; *$p < 0.05$.

the 6-OHDA lesion was similar in PBS-loaded CD163-targeted LCLs or PBS-untargeted LCLs (data not shown), therefore, we used the last one as a control. The Dexa doses were chosen based on our own previous study in rats, where we showed that 0.02 mg of CD163-targeted Dexa/kg was as efficient as 1.0 mg of free Dexa/kg at decreasing the LPS-induced TNF$\alpha$ release (Graversen et al., 2012).

### Glucocorticoid side effect alleviation using liposome encapsulation of Dexa

One of the major advantages of our approach is that, by targeting specifically the CD163 population, the dose needed is substantially lower than the normal Dexa doses used otherwise for anti-inflammatory purposes; doses reported in the literature range from 0.1 to 10 mg/kg (Quan et al., 2014). First, the barrier of polyethylene glycol has been used to ensure that the LCLs are not bound by opsonins and do not inhibit unspecific uptake in phagocytic cells (Allen and Hansen, 1991). Second, we have shown before that coating with polyethylene-glycol-linked anti-CD163 antibodies or drug targeting via the ED2-anti-CD163 antibody ensures fast uptake in CD163+ cells (Etzerodt et al., 2012; Graversen et al., 2012). All of these reduce the dose and therefore the undesired side effects of a chronic treatment. To analyze the side effects commonly observed with prolonged corticoid treatments, we measured the endogenous serum cortisol level and monitored body weight, which decreases in rodents after chronic glucocorticoid treatment (Liu et al., 2011). In addition, we measured thymus size, a commonly used parameter in rodent studies because it reflects the corticosteroid-mediated apoptosis of lymphocytes, dominating cells type of the thymus (Ben Rhouma and Sakly, 1994; Cole et al., 2000). As expected, animals receiving free Dexa showed a significant reduction in all three markers compared with PBS-LCL animals, which did not received any Dexa ($p < 0.001$; Fig. 5). Animals receiving Dexa in targeted or untargeted liposomes were not different from PBS-LCL animals, confirming that the reduction of the dose achieved by the targeting decreased the undesired side effects of the drug.

### CD13-targeted Dexa alleviates motor defects

During the third week of treatment and after surgery, the animals were tested for motor performance using the cylinder test. As a result of the dopaminergic unilateral 6-OHDA neurodegeneration, all animals showed a biased use of the ipsilateral paw versus the lesioned ipsilateral one. However, animals that received ED2-

LCL-Dexa showed significantly better use of the contralateral paw compared with the LCL-PBS control animals. Free Dexa treatment or untargeted Dexa-loaded liposomes did not result in a better motor performance (Fig. 6) This supports a protective ability of the treatment with CD163-targeted liposomes.

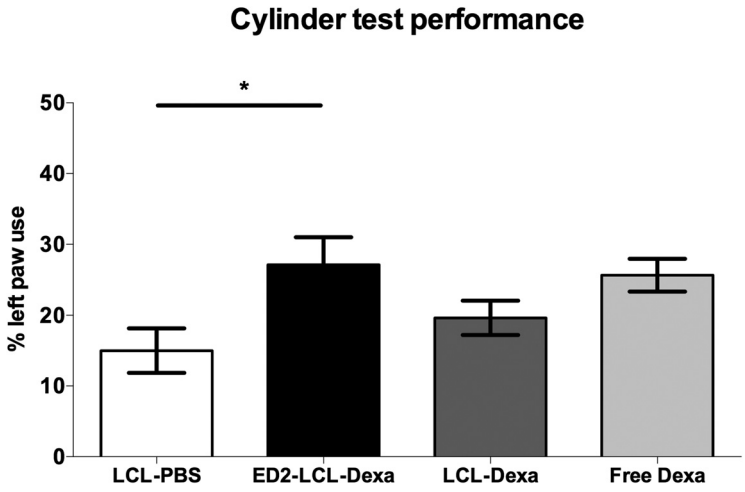



**Figure 6.** Motor performance after striatal 6-OHDA. Spontaneous forelimb use was evaluated by the cylinder test after 3 weeks of treatment. Animals receiving ED2-LCL-Dexa showed better use of the contralateral paw than animals receiving LCL-PBS. Values are expressed as use of the left paw as a percentage of the total: mean ± SEM ($n = 13–14$). One-way ANOVA followed by Tukey *post hoc* analysis: $^*p < 0.05$.

### CD163-targeted glucocorticoid treatment protects dopaminergic nigral neurons

To analyze the status of the dopaminergic nigrostriatal system, we measured the striatal TH+ fiber innervation by densitometric analysis. All groups showed a decrease of the dopaminergic innervation in the ispsilateral striatum 3 weeks after surgery. Although there was a slightly higher density of TH+ fibers in the ED2-LCL-Dexa, no significant difference was found upon statistical analysis (one-way ANOVA, $F_{(3,20)} = 1.288$ $p = 0.30$; Fig. 7). To analyze whether, despite the lack of protection of dopaminergic terminals, we had a change in neuronal survival, we did stereological quantification of the number of TH+ neurons in SN 3 weeks after surgery. The animals receiving ED2-LCL-Dexa had indeed a significant higher number of surviving TH+ neurons compared with those receiving free Dexa or control LCL-PBS (Fig. 8*A–L*). Therefore, Dexa, when targeted to macrophages expressing CD163, could protect dopaminergic neurons, whereas treatment with free Dexa or nontargeted LCL-Dexa did not achieve similar neuroprotection.

### Biochemical analysis of striatal DA metabolism

To analyze the effect of the treatment on DA metabolism, we performed biochemical analysis of DA and metabolites in striatum and SN 3 weeks after surgery by HPLC. We observed a similar profile to that observed upon densitometric analysis of dopaminergic terminals mentioned above, with the highest striatal DA content in the animals receiving ED2-LCL-Dexa, even though it did not reach significant difference (one-way ANOVA, $F_{(3,26)} = 2.420$ $p = 0.089$; Fig. 9*A*). The levels of HVA and DOPAC and the turnover ratios indicated an increase in DA turnover in the 6-OHDA-injected side compared with the contralateral side in all groups except in the ED2-LCL-Dexa animals (Fig. 9*G–I*). No change was observed in the DA, DOPAC, or HVA content in SN and the turnover did not show any signs of significant changes (one-way ANOVA, $F_{(3,22)} = 1.851$, $p = 0.168$; Fig. 9*D–F*, *J–L*).

### CD163-targeted liposomes loaded with low doses of Dexa induced MHCII expression in nigral microglia

As expected, we observed a significant increase in the number of microglia CD11b+ cells in the ipsilateral side in all groups (Fig. 10*A*). However, no difference of the ipsilateral microgliosis was noticed between the CD163 liposomes loaded with Dexa and the control treatments (Fig. 10*B*). Therefore, our treatment did not avoid the proliferation (or recruitment) of microglia induced by 6-OHDA. We analyzed the expression of the CD68 phagocytic marker in our samples. As described previously, we observed upregulation of the protein in the ipsilateral SN, but no obvious difference was found among groups (data not shown).

We also studied the phenotypic changes in activated microglia by quantifying the number of MHCII-expressing microglia in a single representative SN section. As expected, MHCII+ cells were only seen occasionally in the contralateral side of the 6-OHDA lesion at the level of the SN regardless of any treatment. However, MHCII+ cells were densely stained with an activated hyperramified morphology on the ipsilateral side of the 6-OHDA lesion (Fig. 11*A–D*). Animals that received ED2-LCL-Dexa treatment had a significantly higher number of MHCII+ cells compared with the free Dexa group, although animals receiving LCL-Dexa also had elevated MHCII+ cells in SN (Fig. 11*E*). Interestingly, when we plotted and analyzed neuronal dopaminergic survival versus MHCII+ microglia in the SN, we observed a clear trend of positive correlation ($p = 0.06$). Indeed, animals showing an elevated number of surviving TH+ cells also exhibited higher numbers of MHCII+ microglia in SN, but only in the ED2-LCL-Dexa group, not in any of the other groups (Fig. 11*F*).

At the striatal level, all animals showed a robust upregulation of MHCII expression in microglia. When we analyzed the area covered by MHCII+ cells in striatal sections, we observed that animals receiving ED2-LCL-Dexa and LCL-Dexa showed a more widespread MHCII+ cell distribution (Fig. 12*B*, *C*) versus the dense, delimitated area covered by MHCII+ cells in the control groups (Fig. 12*A*, *D*).

## Discussion

We report here that the CD163+ macrophage population significantly infiltrates the neurodegenerating striatal parenchyma in the 6-OHDA PD model. We also show that neuroprotection can be achieved by targeting the infiltrating CD163+ cells using the anti-inflammatory drug Dexa. To do so, we specially designed liposomes targeted for the CD163 and loaded with glucocorticoids. We show that the CD163-targeted-liposomes reached the brain parenchyma, which may occur directly (CD163+ PVM) or indirectly via CD163+-recruited cells. Repeated intravenous injections of these liposomes in the 6-OHDA rats resulted in better motor performance and higher dopaminergic survival. This neuroprotection was observed mainly at the SN, where we also found a significant microgliosis. However, the microglia response appeared different, with a significantly higher number of MHCII+ cells that correlated positively with the neuronal survival. Our

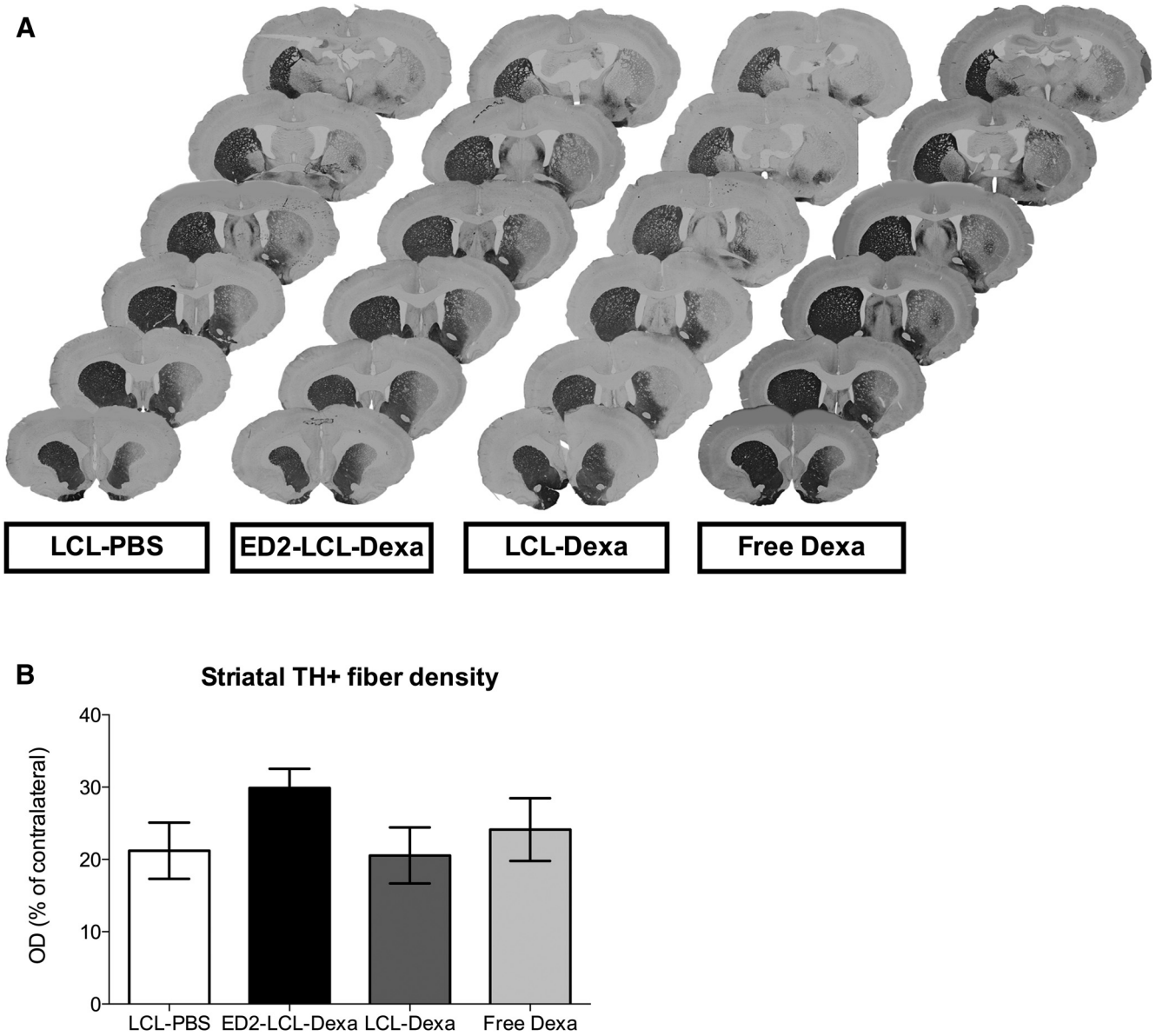



**Figure 7.** Dopaminergic fiber innervation in striatum. ***A***, Photomicrographs showing representative TH-immunostained striatal section in each group 3 weeks after 6-OHDA lesion. ***B***, Bar graph illustrating the semiquantitative measurement of the TH+ densitometry expressed as the percentage of the contralateral side striatal; no significant change was found between groups. Values are mean ± SEM ($n = 6–9$). One-way ANOVA followed by Tukey *post hoc* analysis.

data suggest that modifying the CD163 population by peripheral injections of ED2-LCL loaded with Dexa induces a specific immune response, which results in a distinctive microglial response in the brain correlating with decreased dopaminergic cell death and better motor performance.

We observed a distinguishable increase in the number of CD163+ cells in the lesioned striatum 3 weeks after 6-OHDA. This was not just a consequence of blood–brain barrier damage during surgery because sham surgery did not result in similar increases. Previously, CD163 was defined as the scavenger receptor in monocytes/macrophages responsible for the hemoglobin–haptoglobin complex uptake (Kristiansen et al., 2001). CD163 changes during inflammation and seems related to wound healing (Kowal et al., 2011; Liu et al., 2015). As described, we found that CD163 expression was normally confined to meningeal macrophages (data not shown) and PVM (Polfliet et al., 2006). In healthy rat brain, only occasional CD163+ cells appear in the parenchyma; however, this was significantly increased in the 6-OHDA-lesioned striatum. CD163+ microglia-like cells were reported in certain brain lesion models, although it is unclear whether these cells were of peripheral origin (Zhang et al., 2012). To address whether peripheral CD163+ cells could be recruited to the brain parenchyma, we performed adoptive transfer of CD163+ peritoneal macrophages in 6-OHDA rats. *Ex vivo* labeling of the CD163+ macrophages allowed us to follow them *in vivo* and confirmed their infiltration from the periphery to the brain parenchyma. This is consistent with previous reports documenting infiltration of macrophages, but also T cells, in different neurodegenerative models including PD (Kurkowska-Jastrzebska et al., 1999; Kokovay and Cunningham, 2005; Simard et al., 2006; Rodriguez et al., 2007; Depboylu et al., 2012; Theodore and Maragos, 2015). These infiltrated macrophages may acquire later microglia characteristics (Simard and Rivest, 2004). This recruitment into the area of neurodegeneration seems to happen before cell death, but persists after this occurs (Rodriguez et al., 2007). We saw a significant

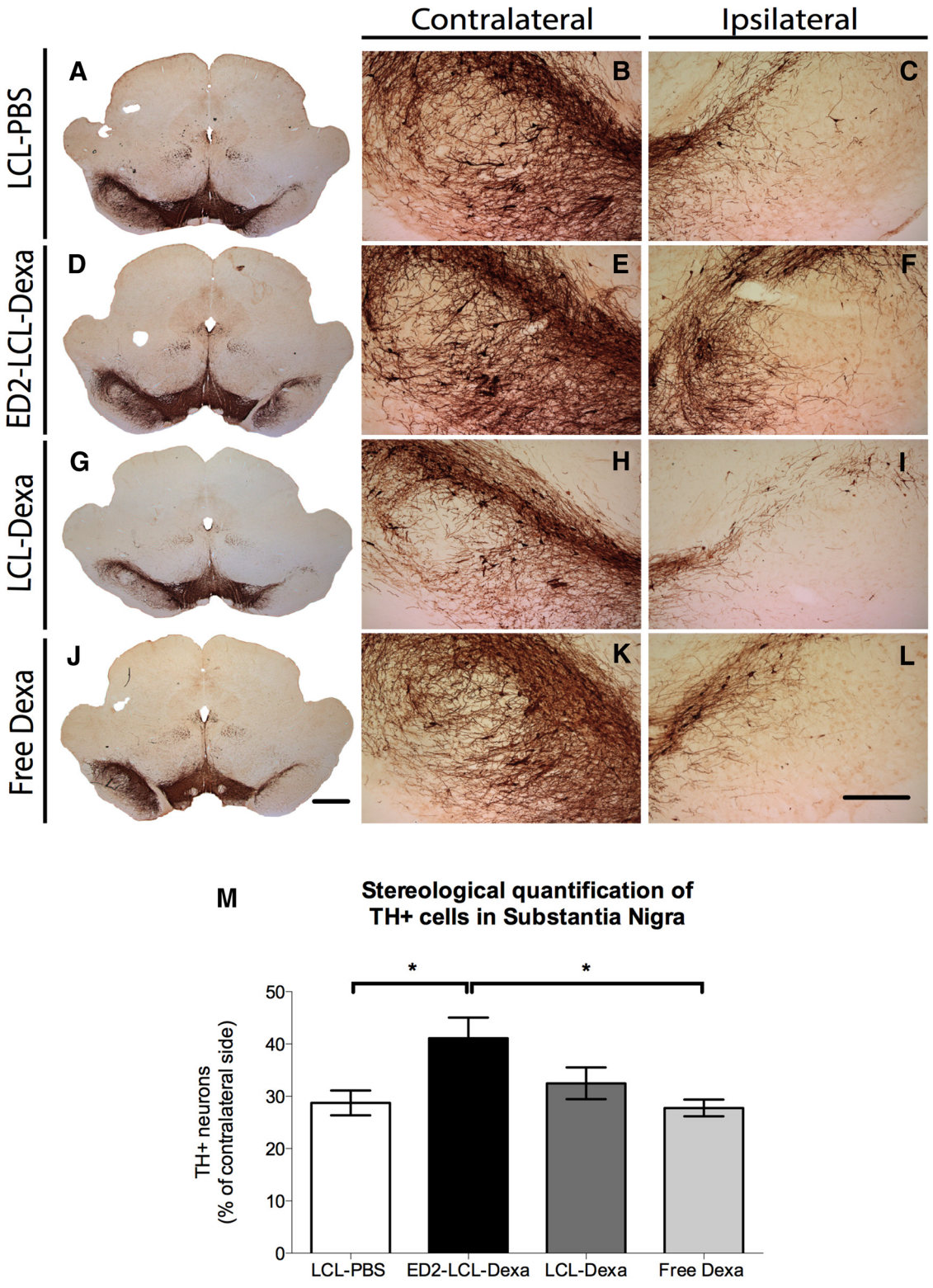



**Figure 8.** Dopaminergic neuronal population in SN. ***A***, ***D***, ***G***, ***J***, Low-magnification photographs showing representative nigral sections immunostained for TH. ***B***, ***C***, ***E***, ***F***, ***H***, ***I***, ***K***, ***L***, Higher magnification of SN from the naive (contralateral) and 6-OHDA (ipsilateral) sides of each section. Notice the higher density of TH+ neurons in the ipsilateral SN in the ED2-LCL-Dexa animal compared with the LCL-PBS or free Dexa animals. ***L***, Bar graphs illustrating the average number of surviving TH+ nigral neurons obtained by stereological quantification expressed as a percentage of the contralateral side. Animals treated with ED2-LCL-Dexa showed higher number of TH+ neurons compared with the ones treated with LCL-PBS or free Dexa. Scale bar in ***J***, 12.5 mm and applies to ***A***, ***D***, ***G***, and ***J***; scale bar in ***L***, 200 $\mu$m and applies to ***B***, ***C***, ***E***, ***F***, ***H***, ***I***, ***K***, and ***L***. Values are mean ± SEM ($n = 12–14$). One-way ANOVA followed by Tukey *post hoc* analysis: *$p < 0.05$.

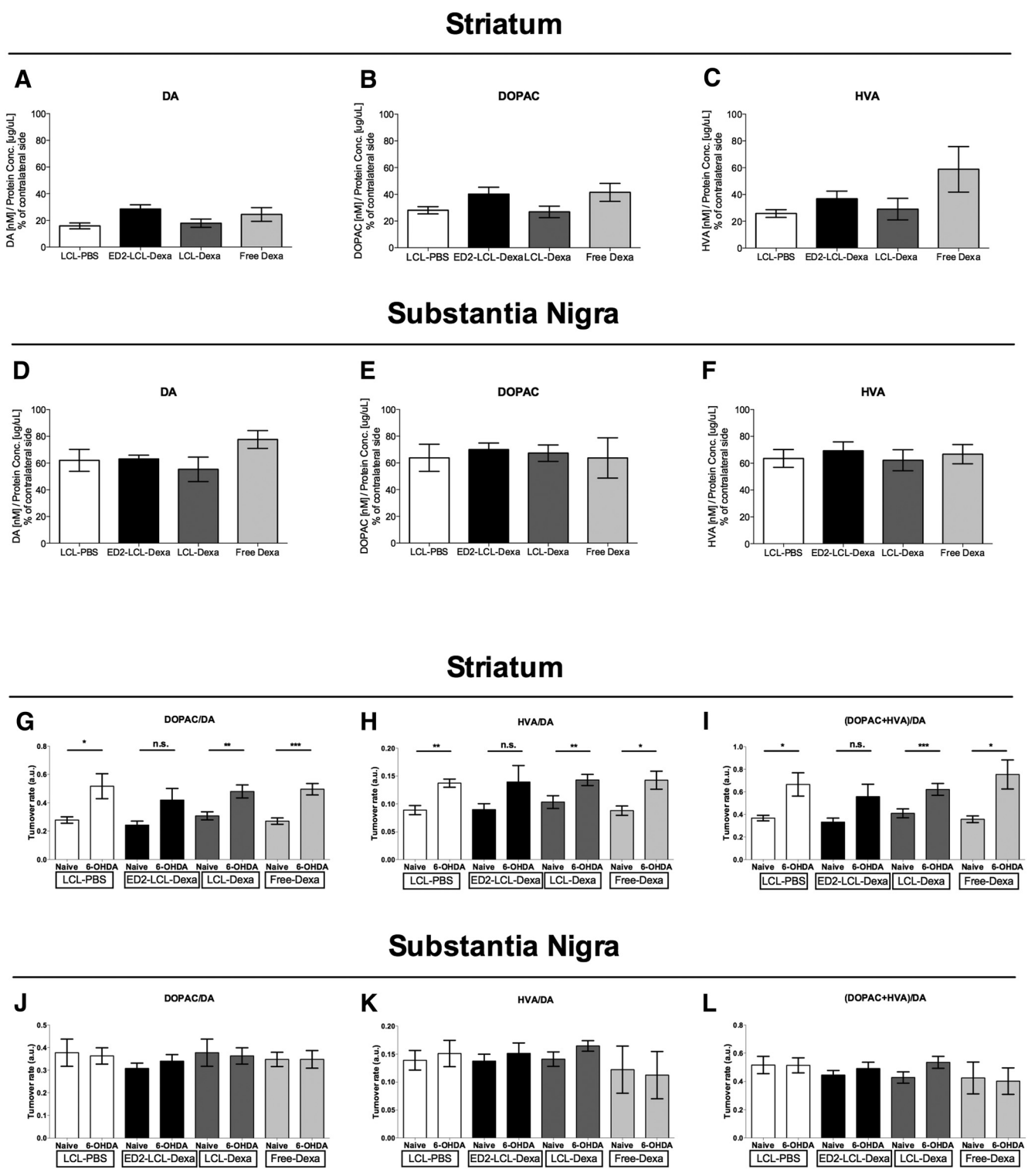



**Figure 9.** Analysis of DA and its metabolites and DA turnover rates. Levels of DA and its metabolites, DOPAC and HVA, were examined by HPLC in the striatum (***A***–***C***) and SN (***D***–***F***) of animals treated for 3 weeks. All animals showed an overt decrease of DA in the lesioned ipsilateral striatum; ED2-LCL-Dexa animals exhibited the highest striatal DA content, but this did not reach significant different (one-way ANOVA, $F_{(3,26)} = 2420$ $p = 0.089$). The turnover of DA was calculated as the DOPAC/DA (***G***, ***J***), HVA/DA (***H***, ***K***), and (DOPAC+HVA)/DA (***I***, ***L***) and examined in the striatum (***G***–***E***) and SN (***J***–***L***) of animals treated for 3 weeks with ED2-LCL-Dexa and control treatments. All animals showed a significant increase in all turnover ratios in the ipsilateral striatum except the ED2-LCL-Dexa animals. No changes were observed in the SN. Values are mean ± SEM ($n = 6–8$). Paired *t* test (contralateral vs ipsilateral) and one-way ANOVA (across groups): $^{***}p < 0.001$; $^{**}p < 0.01$; $^{*}p < 0.05$.

increase of CD163+ after 3 weeks, when cell death had occurred, although our data may suggest that the infiltration could be initiated as soon as 1 week aftersurgery. The role of the infiltrated cells is unclear, but has been proposed to be deleterious based on their iNOS expression (Kokovay and Cunningham, 2005) or protective based on their GDNF expression (Rodriguez et al., 2007). In stroke, the infiltrated cells express protein characteristics of both pro-inflammatory and anti-inflammatory profiles, although their pre-

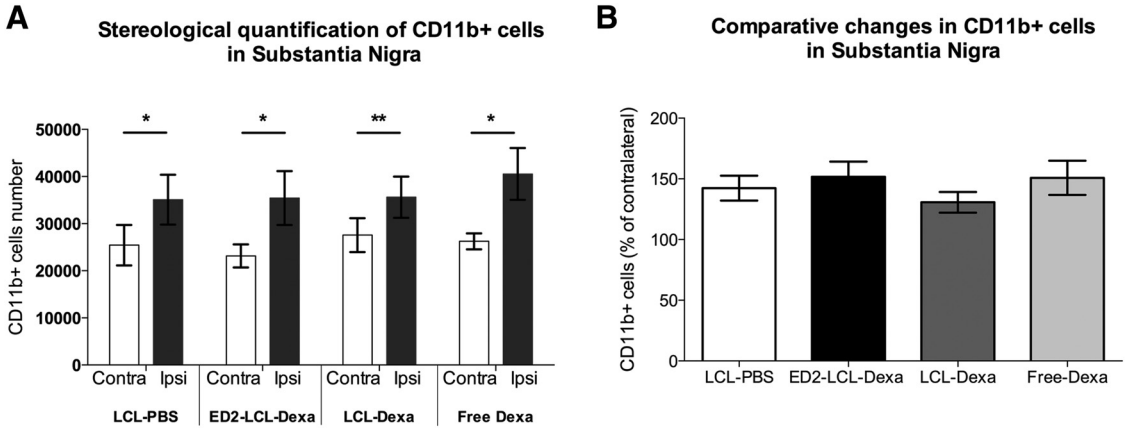



**Figure 10.** Cd11b+ microglia population in the SN. ***A***, Bar graph shows the average number of total cells obtained by stereological quantification of CD11b+ cells both in the contralateral and ipsilateral SN after 3 weeks of treatment. Injection of 6-OHDA in the striatum induced a significant increase of CD11b+ population in the SN regardless of the treatments. ***B***, Bar graphs representing the CD11b+ population in the ipsilateral side expressed as a percentage of the contralateral side showing that no significant difference was found. Values are mean ± SEM ($n = 8$). Paired *t* test (in ***A***) and one-way ANOVA followed by Tukey *post hoc* analysis (***B***).

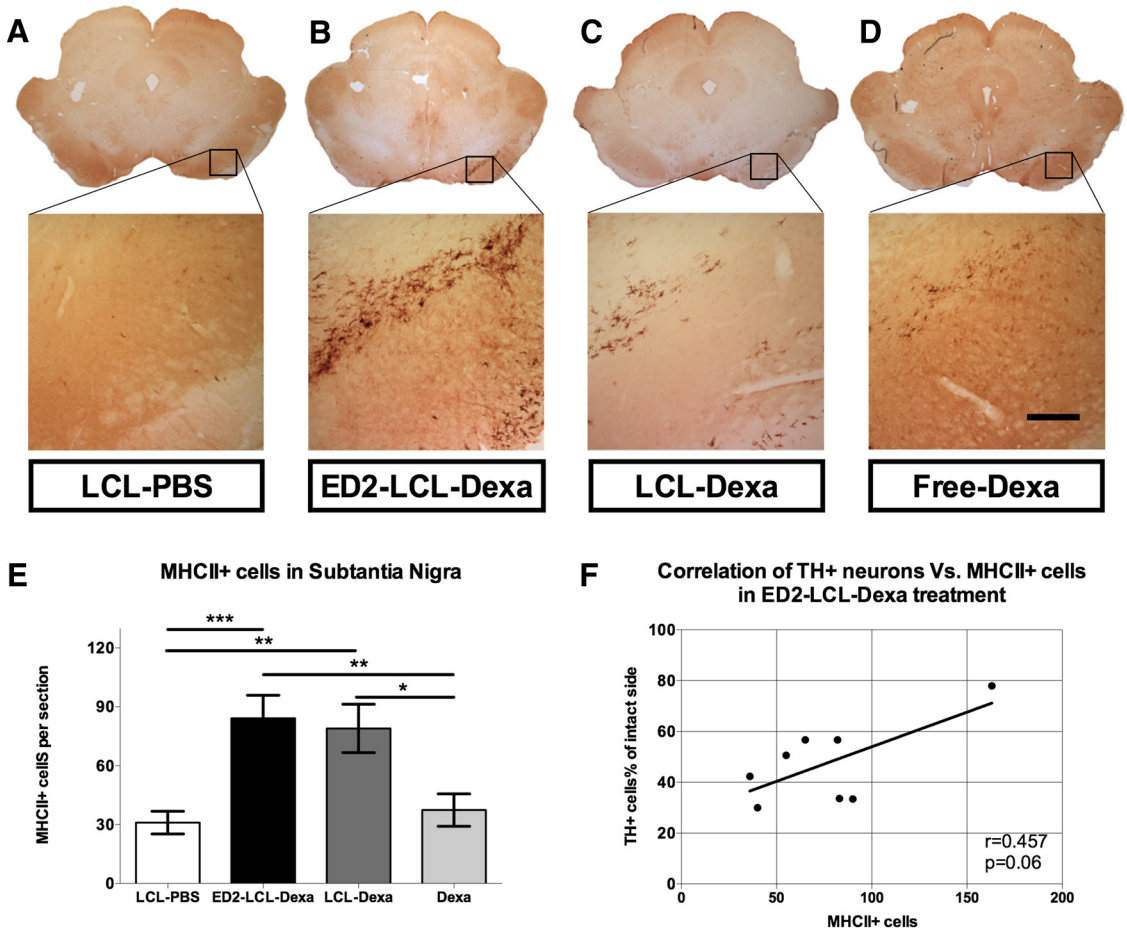



**Figure 11.** MHCII+ microglia in SN. ***A–D***, Low-magnification photos showing representative SN sections immunostained against MHCII from each group. High-power photomicrographs showing insets illustrated in the top low-magnification photos. Notice the higher density of MHCII+ cells in the ipsilateral SN from the animal treated with ED2-LCL-Dexa compared with the ones treated with LCL-PBS or free Dexa. ***E***, Bar graph showing the mean number of MHCII+ cells in ipsilateral SN expressed as a total number of cells per nigral section. Animals treated with ED2-LCL-Dexa and untargeted LCL-Dexa showed an increased number of MHCII+ cells compared with the PBS-LCL control group. ***F***, Positive correlation in between TH+ neurons and MHCII+ cells in SN in ED2-LCL-Dexa-treated animals. Scale bar in ***D***, 200 $\mu$m and applies to high-power photomicrographs in ***A–D***. Values are mean ± SEM ($n = 7–11$). One-way ANOVA followed by Tukey *post hoc* analysis: ***$p < 0.001$; **$p < 0.01$; *$p < 0.05$.

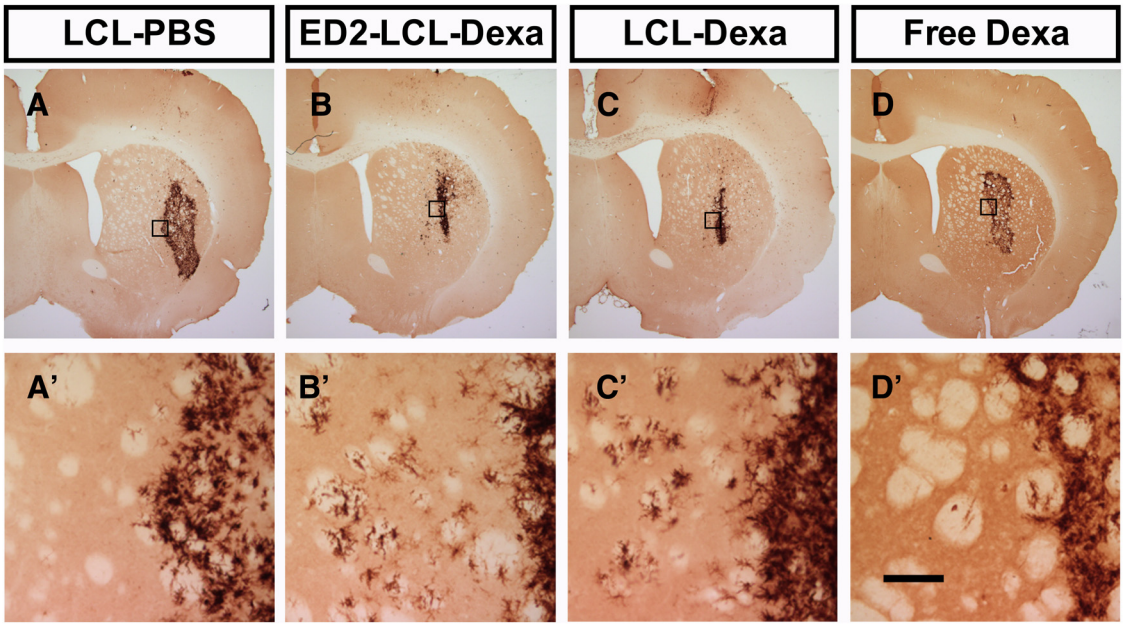



**Figure 12.** MHCII expression in striatum. Photos from striatal section immunostained against MHCII from representative animals of each group 3 weeks after striatal 6-OHDA lesions. Insets indicate areas where the high-power photomicrographs were taken. The animals treated with ED2-LCL-Dexa and LCL-Dexa generally show a smaller area of dense MHCII+ cells at the needle track area, composed of macrophages and or ramified microglia (***B***, ***C***). Notice that the MHCII+ expression was not confined only to the core, but we observed MHCII+ cells spread throughout the striatum (***B′***, ***C′***, insets). LCL-PBS- and free-Dexa-treated animals normally showed a bigger but less dense core covered by MHCII expression associated with the injection area (***A***, ***D***), but the MHCII+ population seemed contained and did not spread through the striatal parenchyma (***A′***, ***D′***, insets). Scale bar, 100 $\mu$m and applies to low-magnification photos.

dominance varied with time (Miro-Mur et al., 2016; Wattananit et al., 2016). In Alzheimer's disease, infiltrated macrophages were related to plaque control (Simard et al., 2006). Intranasal delivery of bone-marrow-derived stem cells resulted in their migration, mainly to the 6-OHDA-lesioned side, accompanied by partial dopaminergic neuroprotection (Danielyan et al., 2011). A similar approach in a transgenic PD model resulted in migration of cells with the ability to phagocyte $\alpha$-synuclein, also suggesting a protective role (Danielyan et al., 2014). Therefore, the role of the infiltrated immune cells in neurodegenerative disease seems complex, with both deleterious and protective phenotypes occurring, probably based on local and peripheral cues. In this context, the role of CD163+ cells is unclear, but its expression is generally considered a sign of an M2 alternative phenotype (Van Gorp et al., 2010). In humans and monkeys, CD163+ microglia-like cells appear in brain upon virus infections, trauma lesions, and immune-related neurodegeneration (Borda et al., 2008; Holfelder et al., 2011). CD163+ cells were observed close to A$\beta$ plaques in Alzheimer's disease patients' brains, suggesting a role for this population in protein aggregation-related neurodegeneration (Zhang et al., 2011; Pey et al., 2014).

We observed that modulation of the immune response via ED2-LCL results in significant protection of dopaminergic neurons and improved motor behavior. Our hypothesis was that the inflammatory event was actively participating in the neurodegenerative process and therefore its modulation would result in protection. We observed here a robust ipsilateral microgliosis 3 weeks after surgery, as described previously (Marinova-Mutafchieva et al., 2009; Virgone-Carlotta et al., 2013; Schlachetzki et al., 2014). CD68 expression suggests that microglial phagocytic activity precedes neuronal death that might be detrimental for dopaminergic survival (Marinova-Mutafchieva et al., 2009). Accordingly, anti-inflammatory strategies are neuroprotective in PD models, such as minocycline or Dexa treatments in the MPTP model (Wu et al., 2002; Kurkowska-Jastrzebska et al., 2004), as well as approaches decreasing pro-inflammatory mediators such as TNF (McCoy et al., 2011) and IL-1beta (Koprich et al., 2008; Pott Godoy et al., 2008; Tanaka et al., 2013). However, therapeutic strategies targeting peripheral macrophages have rarely been used before in PD. *Ex vivo*-modified bone marrow stem cells or macrophages overexpressing GDNF showed neuroprotection in the MPTP and the 6-OHDA models (Biju et al., 2010; Zhao et al., 2014). Nano-formulated catalase administered intravenously after acute MPTP intoxication resulted in protection in SN (Brynskikh et al., 2010); in addition, intravenous transfer of *ex vivo*-transfected macrophages with a catalase plasmid DNA induced neuroprotection in the 6-OHDA model (Haney et al., 2013). Intranasal delivery of bone-marrow-derived stem cells has resulted in new macrophage-like cells in brain associated with neuroprotection (Danielyan et al., 2010; Danielyan et al., 2011; Danielyan et al., 2014). Therefore, targeting peripheral macrophages seems to be a promising tool for neuroprotective therapies.

In our animals, we observed neuronal protection, but no significant protection of the striatal terminals. This could be due to the lesion design and the microglia/immune response time line. Indeed, the 6-OHDA model is a retrograde neurodegenerative model, in which the degeneration is initiated in the terminals and progresses retrogradely toward the nigral cell body. Therefore, the striatal fiber loss starts as soon as 6 h after injection and is accompanied by a rapid and robust microgliosis (Walsh et al., 2011; Stott and Barker, 2014). Although microglia change in profile and protein expression is observed as early as 72 h in SN, the microglia proliferation is delayed 1 week after lesion, at the same time as neurons show the first sign of caspase-3 activation and death (Walsh et al., 2011; Stott and Barker, 2014). This may result in a better window for neuroprotection of the cell bodies using our therapeutic strategy.

Remarkably, we observed microgliosis in SN despite the significant dopaminergic survival, suggesting a modulation of the immune response toward a neuroprotective type without avoiding its proliferation or recruitment. Microglia, as macrophages, have different activation stages: pro-inflammatory, anti-

inflammatory, and repairing. The dynamic response of this population will be determinant for the neuronal fate in PD (Moehle and West, 2015). Others and we have shown previously that microgliosis can occur in the absence of cell death and is associated with neuroprotection (McCoy et al., 2006; Sanchez-Guajardo et al., 2010; Sanchez-Guajardo et al., 2013b). In agreement with our previous observations, we saw increased MHCII expression in the animals in which we observed neuroprotection (Sanchez-Guajardo et al., 2010; Sanchez-Guajardo et al., 2013b). MHCII expression is elevated in microglia in PD patients and is associated with α-synuclein deposition (Croisier et al., 2005). Remarkably, genetic variances related to the MHCII complex in humans are correlated to PD, suggesting a key role for such proteins (Hamza et al., 2010; Wissemann et al., 2013). Increased MHCII has been correlated to neuroprotection upon CX3CL1 overexpression in the 6-OHDA model (Nash et al., 2015). Conversely, in an α-synuclein viral-vector-based PD model, lack of MHCII expression was protective; however, the MHCII knockout line used in the study presents a dramatic decrease of the CD4+ T-cell population, thus complicating the interpretation (Madsen et al., 1999; Harms et al., 2013). MHCII is involved in the presentation of antigens to T cells in adaptive immunity. The adaptive immune system has been also linked to the 6-OHDA PD model and, in the MPTP model, CD4+ T cells are proposed to be essential in neurodegeneration (Brochard et al., 2009; Wheeler et al., 2014; Theodore and Maragos, 2015). Interestingly, although we also observed MHCII upregulation in untargeted LCL-Dexa animals, they did not show neuronal protection, suggesting that the targeting of the LCL to the CD163+ population was key in this therapeutic event. We do not yet know whether the differences reside in changes at the peripheral level or in brain. Therefore, the observation requires further investigation to understand its significance in neuroprotection.

Our results show that peripherally injected nanoparticles targeted to the CD163 receptor can be used to modify the local CNS microglia phenotype significantly and achieve neuroprotection of dopaminergic neurons in a 6-OHDA model of PD. At this point, we cannot discard a protection accomplished through soluble mediators induced by peripheral changes. Nor we can reject the possibility that the liposomes were taken up directly by CD163+ PVM in the brain. However, our data also suggest that a CD163 macrophage population is involved in PD-like neurodegeneration, notably by infiltrating the brain parenchyma. The exact role of these cells and the mechanisms of infiltration into the brain parenchyma are still unclear. The results of our study support the use of targeted glucocorticoids for the treatment of chronic brain inflammation, but stress the importance of characterizing the time course and the associated role of the CD163+ cell population in the degenerative process.

## References


Allen TM, Hansen C (1991) Pharmacokinetics of stealth versus conventional liposomes: effect of dose. Biochim Biophys Acta 1068:133–141. CrossRef Medline

Banati RB, Daniel SE, Blunt SB (1998) Glial pathology but absence of apoptotic nigral neurons in long-standing Parkinson's disease. Mov Disord 13:221–227. CrossRef Medline

Ben Rhouma K, Sakly M (1994) Involution of rat thymus: characterization of cytoplasmic glucocorticoid receptors, evidence of glucocorticoid resistant dexamethasone receptor-positive cells. Arch Int Physiol Biochim Biophys 102:97–102. Medline

Biju K, Zhou Q, Li G, Imam SZ, Roberts JL, Morgan WW, Clark RA, Li S (2010) Macrophage-mediated GDNF delivery protects against dopaminergic neurodegeneration: a therapeutic strategy for Parkinson's disease. Mol Ther 18:1536–1544. CrossRef Medline

Blandini F (2013) Neural and immune mechanisms in the pathogenesis of Parkinson's disease. J Neuroimmune Pharmacol 8:189–201. CrossRef Medline

Borda JT, Alvarez X, Mohan M, Hasegawa A, Bernardino A, Jean S, Aye P, Lackner AA (2008) CD163, a marker of perivascular macrophages, is up-regulated by microglia in simian immunodeficiency virus encephalitis after haptoglobin-hemoglobin complex stimulation and is suggestive of breakdown of the blood-brain barrier. Am J Pathol 172:725–737. CrossRef Medline

Brochard V, Combadière B, Prigent A, Laouar Y, Perrin A, Beray-Berthat V, Bonduelle O, Alvarez-Fisher D, Callebert J, Launay JM, Duyckaerts C, Flavell RA, Hirsch EC, Hunot S (2009) Infiltration of CD4+ lymphocytes into the brain contributes to neurodegeneration in a mouse model of Parkinson disease. J Clin Invest 119:182–192. CrossRef Medline

Brynskikh AM, Zhao Y, Mosley RL, Li S, Boska MD, Klyachko NL, Kabanov AV, Gendelman HE, Batrakova EV (2010) Macrophage delivery of therapeutic nanozymes in a murine model of Parkinson's disease. Nanomedicine (Lond) 5:379–396. CrossRef Medline

Castaño A, Herrera AJ, Cano J, Machado A (2002) The degenerative effect of a single intranigral injection of LPS on the dopaminergic system is prevented by dexamethasone, and not mimicked by rh-TNF-alpha, IL-1beta and IFN-gamma. J Neurochem 81:150–157. CrossRef Medline

Cebrián C, Loike JD, Sulzer D (2015) Neuroinflammation in Parkinson's disease animal models: a cell stress response or a step in neurodegeneration? Curr Top Behav Neurosci 22:237–270. CrossRef Medline

Cicchetti F, Brownell AL, Williams K, Chen YI, Livni E, Isacson O (2002) Neuroinflammation of the nigrostriatal pathway during progressive 6-OHDA dopamine degeneration in rats monitored by immunohistochemistry and PET imaging. Eur J Neurosci 15:991–998. CrossRef Medline

Clerc S, Barenholz Y (1995) Loading of amphipathic weak acids into liposomes in response to transmembrane calcium acetate gradients. Biochim Biophys Acta 1240:257–265. CrossRef Medline

Cole MA, Kim PJ, Kalman BA, Spencer RL (2000) Dexamethasone suppression of corticosteroid secretion: evaluation of the site of action by receptor measures and functional studies. Psychoneuroendocrinology 25:151–167. CrossRef Medline

Croisier E, Moran LB, Dexter DT, Pearce RK, Graeber MB (2005) Microglial inflammation in the parkinsonian substantia nigra: relationship to alpha-synuclein deposition. J Neuroinflammation 2:14. CrossRef Medline

Danielyan L, Klein R, Hanson LR, Buadze M, Schwab M, Gleiter CH, Frey WH (2010) Protective effects of intranasal losartan in the APP/PS1 transgenic mouse model of Alzheimer disease. Rejuvenation Res 13:195–201. CrossRef Medline

Danielyan L, Schäfer R, von Ameln-Mayerhofer A, Bernhard F, Verleysdonk S, Buadze M, Lourhmati A, Klopfer T, Schaumann F, Schmid B, Koehle C, Proksch B, Weissert R, Reichardt HM, van den Brandt J, Buniatian GH, Schwab M, Gleiter CH, Frey WH 2nd (2011) Therapeutic efficacy of intranasally delivered mesenchymal stem cells in a rat model of Parkinson disease. Rejuvenation Res 14:3–16. CrossRef Medline

Danielyan L, Beer-Hammer S, Stolzing A, Schäfer R, Siegel G, Fabian C, Kahle P, Biedermann T, Lourhmati A, Buadze M, Novakovic A, Proksch B, Gleiter CH, Frey WH, Schwab M (2014) Intranasal delivery of bone marrow-derived mesenchymal stem cells, macrophages, and microglia to the brain in mouse models of Alzheimer's and Parkinson's disease. Cell Transplant 23:S123–S139. Medline

Depboylu C, Stricker S, Ghobril JP, Oertel WH, Priller J, Höglinger GU (2012) Brain-resident microglia predominate over infiltrating myeloid cells in activation, phagocytosis and interaction with T-lymphocytes in the MPTP mouse model of Parkinson disease. Exp Neurol 238:183–191. CrossRef Medline

Doorn KJ, Lucassen PJ, Boddeke HW, Prins M, Berendse HW, Drukarch B, van Dam AM (2012) Emerging roles of microglial activation and non-motor symptoms in Parkinson's disease. Prog Neurobiol 98:222–238. CrossRef Medline

Dultz G, Gerber L, Zeuzem S, Sarrazin C, Waidmann O (2016) The macrophage activation marker CD163 is associated with IL28B genotype and hepatic inflammation in chronic hepatitis C virus infected patients. J Viral Hepat 23:267–273. CrossRef Medline

Etzerodt A, Moestrup SK (2013) CD163 and inflammation: biological, diagnostic, and therapeutic aspects. Antioxid Redox Signal 18:2352–2363. CrossRef Medline

Etzerodt A, Maniecki MB, Graversen JH, Møller HJ, Torchilin VP, Moestrup SK (2012a) Efficient intracellular drug-targeting of macrophages using stealth liposomes directed to the hemoglobin scavenger receptor CD163. J Control Release 160:72–80. CrossRef Medline

Febbraro F, Andersen KJ, Sanchez-Guajardo V, Tentillier N, Romero-Ramos M (2013) Chronic intranasal deferoxamine ameliorates motor defects and pathology in the alpha-synuclein rAAV Parkinson's model. Exp Neurol 247:45–58. CrossRef Medline

Gao HM, Zhang F, Zhou H, Kam W, Wilson B, Hong JS (2011) Neuroinflammation and alpha-synuclein dysfunction potentiate each other, driving chronic progression of neurodegeneration in a mouse model of Parkinson's disease. Environ Health Perspect 119:807–814. CrossRef Medline

Garcia-Esparcia P, Llorens F, Carmona M, Ferrer I (2014) Complex deregulation and expression of cytokines and mediators of the immune response in Parkinson's disease brain is region dependent. Brain Pathol 24:584–598. CrossRef Medline

Paxinos G, Watson C (1998) The rat brain in stereotaxic coordinates. San Diego: Academic.

Gerhard A, Pavese N, Hotton G, Turkheimer F, Es M, Hammers A, Eggert K, Oertel W, Banati RB, Brooks DJ (2006) In vivo imaging of microglial activation with [11C](R)-PK11195 PET in idiopathic Parkinson's disease. Neurobiol Dis 21:404–412. CrossRef Medline

Graversen JH, Svendsen P, Dagnæs-Hansen F, Dal J, Anton G, Etzerodt A, Petersen MD, Christensen PA, Møller HJ, Moestrup SK (2012a) Targeting the hemoglobin scavenger receptor CD163 in macrophages highly increases the anti-inflammatory potency of dexamethasone. Mol Ther 20:1550–1558. CrossRef Medline

Hamza TH, Zabetian CP, Tenesa A, Laederach A, Montimurro J, Yearout D, Kay DM, Doheny KF, Paschall J, Pugh E, Kusel VI, Collura R, Roberts J, Griffith A, Samii A, Scott WK, Nutt J, Factor SA, Payami H (2010) Common genetic variation in the HLA region is associated with late-onset sporadic Parkinson's disease. Nat Genet 42:781–785. CrossRef Medline

Haney MJ, Zhao Y, Harrison EB, Mahajan V, Ahmed S, He Z, Suresh P, Hingtgen SD, Klyachko NL, Mosley RL, Gendelman HE, Kabanov AV, Batrakova EV (2013) Specific transfection of inflamed brain by macrophages: a new therapeutic strategy for neurodegenerative diseases. PLoS One 8:e61852. CrossRef Medline

Harms AS, Cao S, Rowse AL, Thome AD, Li X, Mangieri LR, Cron RQ, Shacka JJ, Raman C, Standaert DG (2013) MHCII is required for alpha-synuclein-induced activation of microglia, CD4 T cell proliferation, and dopaminergic neurodegeneration. J Neurosci 33:9592–9600. CrossRef Medline

Herrera AJ, Tomás-Camardiel M, Venero JL, Cano J, Machado A (2005) Inflammatory process as a determinant factor for the degeneration of substantia nigra dopaminergic neurons. J Neural Transm 112:111–119. CrossRef Medline

Holfelder K, Schittenhelm J, Trautmann K, Haybaeck J, Meyermann R, Beschorner R (2011) De novo expression of the hemoglobin scavenger receptor CD163 by activated microglia is not associated with hemorrhages in human brain lesions. Histol Histopathol 26:1007–1017. Medline

Hunot S, Boissière F, Faucheux B, Brugg B, Mouatt-Prigent A, Agid Y, Hirsch EC (1996) Nitric oxide synthase and neuronal vulnerability in Parkinson's disease. Neuroscience 72:355–363. CrossRef Medline

Imamura K, Hishikawa N, Sawada M, Nagatsu T, Yoshida M, Hashizume Y (2003) Distribution of major histocompatibility complex class II-positive microglia and cytokine profile of Parkinson's disease brains. Acta Neuropathol 106:518–526. CrossRef Medline

Joers V, Tansey MG, Mulas G, Carta AR (2016) Microglial phenotypes in Parkinson's disease and animal models of the disease. Prog Neurobiol. In press.

Knott C, Stern G, Wilkin GP (2000) Inflammatory regulators in Parkinson's disease: iNOS, lipocortin-1, and cyclooxygenases-1 and -2. Mol Cell Neurosci 16:724–739. CrossRef Medline

Kokovay E, Cunningham LA (2005) Bone marrow-derived microglia contribute to the neuroinflammatory response and express iNOS in the MPTP mouse model of Parkinson's disease. Neurobiol Dis 19:471–478. CrossRef Medline

Koprich JB, Reske-Nielsen C, Mithal P, Isacson O (2008) Neuroinflammation mediated by IL-1beta increases susceptibility of dopamine neurons to degeneration in an animal model of Parkinson's disease. J Neuroinflammation 5:8. CrossRef Medline

Kowal K, Silver R, Sławińska E, Bielecki M, Chyczewski L, Kowal-Bielecka O (2011) CD163 and its role in inflammation. Folia Histochem Cytobiol 49:365–374. CrossRef Medline

Kristiansen M, Graversen JH, Jacobsen C, Sonne O, Hoffman HJ, Law SK, Moestrup SK (2001) Identification of the haemoglobin scavenger receptor. Nature 409:198–201. CrossRef Medline

Kurkowska-Jastrzebska I, Wrońska A, Kohutnicka M, Członkowski A, Członkowska A (1999) The inflammatory reaction following 1-methyl-4-phenyl-1,2,3, 6-tetrahydropyridine intoxication in mouse. Exp Neurol 156:50–61. CrossRef Medline

Kurkowska-Jastrzebska I, Litwin T, Joniec I, Ciesielska A, Przybyłkowski A, Członkowski A, Członkowska A (2004) Dexamethasone protects against dopaminergic neurons damage in a mouse model of Parkinson's disease. Int Immunopharmacol 4:1307–1318. CrossRef Medline

Liu B, Hu B, Shao S, Wu W, Fan L, Bai G, Shang P, Wang X (2015) CD163/hemoglobin oxygenase-1 pathway regulates inflammation in hematoma surrounding tissues after intracerebral hemorrhage. J Stroke Cerebrovasc Dis 24:2800–2809. CrossRef Medline

Liu XY, Shi JH, Du WH, Fan YP, Hu XL, Zhang CC, Xu HB, Miao YJ, Zhou HY, Xiang P, Chen FL (2011) Glucocorticoids decrease body weight and food intake and inhibit appetite regulatory peptide expression in the hypothalamus of rats. Exp Ther Med 2:977–984. Medline

Lossinsky AS, Shivers RR (2004) Structural pathways for macromolecular and cellular transport across the blood-brain barrier during inflammatory conditions. Histol Histopathol 19:535–564. Medline

Madsen L, Labrecque N, Engberg J, Dierich A, Svejgaard A, Benoist C, Mathis D, Fugger L (1999) Mice lacking all conventional MHC class II genes. Proc Natl Acad Sci U S A 96:10338–10343. CrossRef Medline

Marinova-Mutafchieva L, Sadeghian M, Broom L, Davis JB, Medhurst AD, Dexter DT (2009) Relationship between microglial activation and dopaminergic neuronal loss in the substantia nigra: a time course study in a 6-hydroxydopamine model of Parkinson's disease. J Neurochem 110:966–975. CrossRef Medline

McCoy MK, Martinez TN, Ruhn KA, Szymkowski DE, Smith CG, Botterman BR, Tansey KE, Tansey MG (2006) Blocking soluble tumor necrosis factor signaling with dominant-negative tumor necrosis factor inhibitor attenuates loss of dopaminergic neurons in models of Parkinson's disease. J Neurosci 26:9365–9375. CrossRef Medline

McCoy MK, Ruhn KA, Blesch A, Tansey MG (2011) TNF: a key neuroinflammatory mediator of neurotoxicity and neurodegeneration in models of Parkinson's disease. Adv Exp Med Biol 691:539–540. CrossRef Medline

Miro-Mur F, Perez-de-Puig I, Ferrer-Ferrer M, Urra X, Justicia C, Chamorro A, Planas AM (2016) Immature monocytes recruited to the ischemic mouse brain differentiate into macrophages with features of alternative activation. Brain Behav Immun 53:18–33. CrossRef Medline

Moehle MS, West AB (2015) M1 and M2 immune activation in Parkinson's disease: foe and ally? Neuroscience 302:59–73. CrossRef Medline

Mogi M, Harada M, Riederer P, Narabayashi H, Fujita K, Nagatsu T (1994) Tumor necrosis factor-alpha (TNF-alpha) increases both in the brain and in the cerebrospinal fluid from parkinsonian patients. Neurosci Lett 165:208–210. CrossRef Medline

Mougin-Degraef M, Jestin E, Bruel D, Remaud-Le Saëc P, Morandeau L, Faivre-Chauvet A, Barbet J (2006) High-activity radio-iodine labeling of conventional and stealth liposomes. J Liposome Res 16:91–102. CrossRef Medline

Na SJ, DiLella AG, Lis EV, Jones K, Levine DM, Stone DJ, Hess JF (2010) Molecular profiling of a 6-hydroxydopamine model of Parkinson's disease. Neurochem Res 35:761–772. CrossRef Medline

Nagatsu T, Sawada M (2005) Inflammatory process in Parkinson's disease: role for cytokines. Curr Pharm Des 11:999–1016. CrossRef Medline

International Parkinson Disease Genomics Consortium, Nalls MA, Plagnol V, Hernandez DG, Sharma M, Sheerin UM, Saad M, Simón-Sánchez J, Schulte C, Lesage S, Sveinbjörnsdóttir S, Stefánsson K, Martinez M, Hardy J, Heutink P, Brice A, Gasser T, Singleton AB, Wood NW (2011) Imputation of sequence variants for identification of genetic risks for Parkinson's disease: a meta-analysis of genome-wide association studies. Lancet 377:641–649. CrossRef Medline

Nash KR, Moran P, Finneran DJ, Hudson C, Robinson J, Morgan D, Bickford PC (2015) Fractalkine over expression suppresses alpha-synuclein-mediated neurodegeneration. Mol Ther 23:17–23. CrossRef Medline

Ouchi Y, Yoshikawa E, Sekine Y, Futatsubashi M, Kanno T, Ogusu T, Tori-

zuka T (2005) Microglial activation and dopamine terminal loss in early Parkinson's disease. Ann Neurol 57:168–175. CrossRef Medline

Pey P, Pearce RK, Kalaitzakis ME, Griffin WS, Gentleman SM (2014) Phenotypic profile of alternative activation marker CD163 is different in Alzheimer's and Parkinson's disease. Acta Neuropathol Commun 2:21. CrossRef Medline

Polfliet MM, Fabriek BO, Daniëls WP, Dijkstra CD, van den Berg TK (2006) The rat macrophage scavenger receptor CD163: expression, regulation and role in inflammatory mediator production. Immunobiology 211: 419–425. CrossRef Medline

Pott Godoy MC, Tarelli R, Ferrari CC, Sarchi MI, Pitossi FJ (2008) Central and systemic IL-1 exacerbates neurodegeneration and motor symptoms in a model of Parkinson's disease. Brain 131:1880–1894. CrossRef Medline

Quan L, Zhang Y, Crielaard BJ, Dusad A, Lele SM, Rijcken CJ, Metselaar JM, Kostkova H, Etrych T, Ulbrich K, Kiessling F, Mikuls TR, Hennink WE, Storm G, Lammers T, Wang D (2014) Nanomedicines for inflammatory arthritis: head-to-head comparison of glucocorticoid-containing polymers, micelles, and liposomes. ACS Nano 8:458–466. CrossRef Medline

Rees K, Stowe R, Patel S, Ives N, Breen K, Clarke CE, Ben-Shlomo Y (2011) Non-steroidal anti-inflammatory drugs as disease-modifying agents for Parkinson's disease: evidence from observational studies. Cochrane Database Syst Rev 11:CD008454. CrossRef Medline

Rodriguez M, Alvarez-Erviti L, Blesa FJ, Rodríguez-Oroz MC, Arina A, Melero I, Ramos LI, Obeso JA (2007) Bone-marrow-derived cell differentiation into microglia: a study in a progressive mouse model of Parkinson's disease. Neurobiol Dis 28:316–325. CrossRef Medline

Sanchez-Guajardo V, Febbraro F, Kirik D, Romero-Ramos M (2010) Microglia acquire distinct activation profiles depending on the degree of alpha-synuclein neuropathology in a rAAV based model of Parkinson's disease. PLoS One 5:e8784. CrossRef Medline

Sanchez-Guajardo V, Barnum CJ, Tansey MG, Romero-Ramos M (2013a) Neuroimmunological processes in Parkinson's disease and their relation to alpha-synuclein: microglia as the referee between neuronal processes and peripheral immunity. ASN Neuro 5:113–139. CrossRef Medline

Sanchez-Guajardo V, Annibali A, Jensen PH, Romero-Ramos M (2013b) alpha-Synuclein vaccination prevents the accumulation of parkinson disease-like pathologic inclusions in striatum in association with regulatory T cell recruitment in a rat model. J Neuropathol Exp Neurol 72: 624–645. CrossRef Medline

Schallert T, Fleming SM, Leasure JL, Tillerson JL, Bland ST (2000) CNS plasticity and assessment of forelimb sensorimotor outcome in unilateral rat models of stroke, cortical ablation, parkinsonism and spinal cord injury. Neuropharmacology 39:777–787. CrossRef Medline

Schlachetzki JC, Marxreiter F, Regensburger M, Kulinich A, Winner B, Winkler J (2014) Increased tyrosine hydroxylase expression accompanied by glial changes within the non-lesioned hemisphere in the 6-hydroxydopamine model of Parkinson's disease. Restor Neurol Neurosci 32: 447–462. CrossRef Medline

Simard AR, Rivest S (2004) Bone marrow stem cells have the ability to populate the entire central nervous system into fully differentiated parenchymal microglia. FASEB J 18:998–1000. Medline

Simard AR, Soulet D, Gowing G, Julien JP, Rivest S (2006) Bone marrow-derived microglia play a critical role in restricting senile plaque formation in Alzheimer's disease. Neuron 49:489–502. CrossRef Medline

Stott SR, Barker RA (2014) Time course of dopamine neuron loss and glial response in the 6-OHDA striatal mouse model of Parkinson's disease. Eur J Neurosci 39:1042–1056. CrossRef Medline

Tanaka S, Ishii A, Ohtaki H, Shioda S, Yoshida T, Numazawa S (2013) Activation of microglia induces symptoms of Parkinson's disease in wild-type, but not in IL-1 knockout mice. J Neuroinflammation 10: 143. CrossRef Medline

Theodore S, Maragos W (2015) 6-Hydroxydopamine as a tool to understand adaptive immune system-induced dopamine neurodegeneration in Parkinson's disease. Immunopharmacol Immunotoxicol 37:393–399. CrossRef Medline

Torchilin VP, Levchenko TS, Lukyanov AN, Khaw BA, Klibanov AL, Rammohan R, Samokhin GP, Whiteman KR (2001) p-Nitrophenylcarbonyl-PEG-PE-liposomes: fast and simple attachment of specific ligands, including monoclonal antibodies, to distal ends of PEG chains via p-nitrophenylcarbonyl groups. Biochim Biophys Acta 1511:397–411. CrossRef Medline

Van Gorp H, Delputte PL, Nauwynck HJ (2010) Scavenger receptor CD163, a Jack-of-all-trades and potential target for cell-directed therapy. Mol Immunol 47:1650–1660. CrossRef Medline

Villarán RF, Espinosa-Oliva AM, Sarmiento M, De Pablos RM, Argüelles S, Delgado-Cortés MJ, Sobrino V, Van Rooijen N, Venero JL, Herrera AJ, Cano J, Machado A (2010) Ulcerative colitis exacerbates LPS-induced damage to the nigral dopaminergic system: potential risk factor in Parkinson'disease. J Neurochem 114:1687–1700. CrossRef Medline

Virgone-Carlotta A, Uhlrich J, Akram MN, Ressnikoff D, Chrétien F, Domenget C, Gherardi R, Despars G, Jurdic P, Honnorat J, Nataf S, Touret M (2013) Mapping and kinetics of microglia/neuron cell-to-cell contacts in the 6-OHDA murine model of Parkinson's disease. Glia 61:1645–1658. CrossRef Medline

Walsh S, Finn DP, Dowd E (2011) Time-course of nigrostriatal neurodegeneration and neuroinflammation in the 6-hydroxydopamine-induced axonal and terminal lesion models of Parkinson's disease in the rat. Neuroscience 175:251–261. CrossRef Medline

Wattananit S, Tornero D, Graubardt N, Memanishvili T, Monni E, Tatarishvili J, Miskinyte G, Ge R, Ahlenius H, Lindvall O, Schwartz M, Kokaia Z (2016) Monocyte-derived macrophages contribute to spontaneous long-term functional recovery after stroke in mice. J Neurosci 36:4182–4195. CrossRef Medline

Westermeyer J (1991) Problems with managed psychiatric care without a psychiatrist-manager. Hosp Community Psychiatry 42:1221–1224. Medline

Wheeler CJ, Seksenyan A, Koronyo Y, Rentsendorj A, Sarayba D, Wu H, Gragg A, Siegel E, Thomas D, Espinosa A, Thompson K, Black K, Koronyo-Hamaoui M, Pechnick R, Irvin DK (2014) T-lymphocyte deficiency exacerbates behavioral deficits in the 6-OHDA unilateral lesion rat model for Parkinson's disease. J Neurol Neurophysiol 5:pii:209. CrossRef Medline

Wissemann WT, Hill-Burns EM, Zabetian CP, Factor SA, Patsopoulos N, Hoglund B, Holcomb C, Donahue RJ, Thomson G, Erlich H, Payami H (2013) Association of Parkinson disease with structural and regulatory variants in the HLA region. Am J Hum Genet 93:984–993. CrossRef Medline

Wu DC, Jackson-Lewis V, Vila M, Tieu K, Teismann P, Vadseth C, Choi DK, Ischiropoulos H, Przedborski S (2002) Blockade of microglial activation is neuroprotective in the 1-methyl-4-phenyl-1,2,3,6-tetrahydropyridine mouse model of Parkinson disease. J Neurosci 22:1763–1771. Medline

Zhang Z, Zhang ZY, Schittenhelm J, Wu Y, Meyermann R, Schluesener HJ (2011) Parenchymal accumulation of CD163+ macrophages/microglia in multiple sclerosis brains. J Neuroimmunol 237:73–79. CrossRef Medline

Zhang Z, Zhang ZY, Wu Y, Schluesener HJ (2012) Lesional accumulation of CD163+ macrophages/microglia in rat traumatic brain injury. Brain Res 1461:102–110. CrossRef Medline

Zhao Y, Haney MJ, Mahajan V, Reiner BC, Dunaevsky A, Mosley RL, Kabanov AV, Gendelman HE, Batrakova EV (2011) Active targeted macrophage-mediated delivery of catalase to affected brain regions in models of Parkinson's disease. J Nanomed Nanotechnol S4:pii:003. CrossRef Medline

Zhao Y, Haney MJ, Gupta R, Bohnsack JP, He Z, Kabanov AV, Batrakova EV (2014) GDNF-transfected macrophages produce potent neuroprotective effects in Parkinson's disease mouse model. PLoS One 9:e106867. CrossRef Medline